The Thesis Committee for Ali Saeed Alqarni
Certifies that this is the approved version of the following thesis:

Quantifying the Characteristics of Fine Aggregate Using Direct and Indirect Test Methods

APPROVED BY
SUPERVISING COMMITTEE:

Supervisor:

David Fowler

Raissa Ferron

Quantifying the Characteristics of Fine Aggregate Using Direct and Indirect Test Methods

by

Ali Saeed Alqarni, B.S.

Thesis

Presented to the Faculty of the Graduate School of

The University of Texas at Austin

in Partial Fulfillment

of the Requirements

for the Degree of

Master of Science in Engineering

The University of Texas at Austin

December 2013

Acknowledgements

I would like to express my gratitude to Dr. David Fowler for giving me the opportunity to work on this project and the guidance he has given to me during it. His expertise, understanding, and patience added considerably to my graduate experience. I cannot imagine having had a better advisor. I would also like to thank Dr. Raissa Ferron for serving as a member of my thesis committee

A very special thank you goes out to Chris Clement, who worked on this project as a PhD student alongside of me. He was always more than happy to help and give advice when needed. The testing performed in this thesis could not have done without his help and support. I would also like to thank everyone around the laboratory, especially Marc Rached, Adrian Saldanha, Md. Sarwar Siddiqui, and Zack Stutts, for their help and support during this project.

I would like to recognize my friends in the USA, Majeed, Talal, Ahmad, Bin Saedy, Hamdan, Yasser, Abdullah, Mohammad, Bader, Abdulaziz, Mohannad and Wes, for their continuous support and encouragement.

Finally, I would like to thank my family for their support throughout my entire life and during this period in particular. I could not have asked for better parents.

Abstract

Quantifying the Characteristics of Fine Aggregate Using Direct and Indirect Test Methods

Ali Saeed Alqarni, M.S.E.

The University of Texas at Austin, 2013

Supervisor: David W. Fowler

Abstract: The characteristics of fine aggregates, such as shape, angularity, and surface texture, have been shown to influence the performance of concrete and asphalt mixtures and to play an important role in obtaining valuable properties of early age concrete such as workability, and compatibility. However, the measurement of fine aggregate characteristics is not easy. In the present study, 26 fine aggregates, covering a wide spectrum of mineralogy, were examined using direct and indirect test methods in order to evaluate the shape, angularity, and surface texture, as well as to analyze the gradation. The direct test methods, such as AIMS and Camsizer, which provide a digital image of the aggregates proved to be the best. However, the cost of such systems can limit the use of digital imagining systems in practice. The indirect test methods which provide an estimate of aggregate surface characteristics, such as uncompacted void test, mortar flow test, compressive strength test, and flakiness test gave variable results. The uncompacted void test (Method A) was shown to be the most accurate indirect test method. The Camsizer and the sieve analysis test produced identical gradation analysis results when an adequate sample was used. General correlations were developed between the direct and indirect test methods. The non-approved fine aggregates on the TxDOT's

list were analyzed and compared to those of the approved fine aggregates to see whether they could be successfully used. It was found that both LS-5 and LS-8 had good results—even better than the results of some of the approved fine aggregates. Thus, they could be successfully used.

Table of Contents

Table of Contents

List of Figures

Chapter 1: Introduction

Fine and coarse aggregates, used in making portland cement concrete as well as asphalt concrete, occupy approximately 70 to 80% of the total volume of the mixture. Fine aggregate is classified as the material passing the 4.75 mm (No. 4) sieve and retained on the 75 μm (No. 200) sieve. The performance of concrete and asphalt mixtures is highly influenced by the characteristics of aggregate e.g. shape, angularity, and surface texture. Several studies have shown that aggregate characteristics have a significant impact on the mechanical properties of portland cement concrete and pavement base layers. Mahmoud, Gates, Masad, Erdogan, and Garboczi (2010) noted that rheology, shrinkage, and durability are mainly affected by the aggregate properties

The characteristics of fine aggregate are generally expressed in terms of shape, angularity, and surface texture. These characteristics play an important role in successfully obtaining excellent properties of early age concrete such as workability, flowability, and compatibility. Furthermore, It has been well documented that the characteristics of fine aggregates play a significant role in rutting resistance of hot-mix asphalt (Topal and Sengoz, 2008). As a result, the Corps of Engineers has limited the amount of natural sand content in asphalt concrete because premature rutting results from having an excessive amount of natural round sand.

The measurement of fine aggregate characteristics is not an easy task. Many organizations have adopted different test methods for evaluating and measuring the characteristics of fine aggregate, some of which are considered to be indirect tests. example of popular indirect tests discussed in the literature are the uncompacted void

content of fine aggregate, the Florida bearing value of fine aggregate, the flakiness sieve, the compacted aggregate resistance (CAR), the University of Illinois aggregate image analyzer (UIAIA), and the Aggregate Imaging System (AIMS). Each of these test methods has advantages and disadvantages. For instance, certain test methods can measure the fine aggregate's characteristics (shape, angularity, and texture), while others evaluate only the shape of fine aggregates. With modern developments in technology, digital imaging systems can be incorporated to automatically measure the shape, angularity, and texture of fine aggregate. However, the cost of such systems can limit the use of digital imaging systems in practice. For example, Masad, Al-Rousan, Button, Little, and Tutumluer (2007) pointed out that the equipment costs of the AIMS and the Camsizer are $35,000 and $45,000, respectively, while the cost of uncompacted void content testing equipment is $250.

The AIMS is used to measure two fine aggregate characteristics, which are form 2-D and angularity. The form two-dimensional images of fine aggregate particles are evaluated and quantified by analyzing the black-and-white image of a particle projection, while the gradient angularity quantifies the change in the gradient within the boundary of each particle. It also determines how sharp the corners of the two-dimensional images of fine aggregate particles are.

The Dynamic Image Analysis System also known as the Camsizer evaluates and measures the shape and angularity of aggregate. In addition, gradation analysis can be automatically conducted on the Camsizer. The Camsizer has two cameras to capture images at different magnifications based on the size of each particle. The characteristics of fine aggregate in the Camsizer are expressed in terms of sphericity and symmetry. The

sphericity, or roundness, is defined as the ratio of the area of a fine aggregate particle to its perimeter, whereas the symmetry evaluates the angularity of each particle. The importance of the symmetry parameter is its ability to identify broken particles within a sample.

The uncompacted void content of fine aggregate method is an indirect test that evaluates the shape and texture characteristics of fine aggregate by comparing the packing densities. The test adopts three different methods, Methods A, B, and C. Method A is called the standard graded sample, and it uses a standard fine aggregate grading achieved by mixing individual sieve fractions from the sieve analysis test of fine aggregate. Method B is called individual size fractions, and it uses three different size fractions. Method B is more time-consuming, since each size fraction has to be tested separately and it requires a larger sample than other methods; however, it yields more information regarding the shape and texture characteristics of each individual size fraction. Method C may be suitable in determining proportions and components used in mixtures.

To measure and evaluate the characteristics of fine aggregate using different tests and techniques, the present study extensively examined 26 fine aggregate specimens covering a wide spectrum of mineralogy, such as dolomite, limestone, sandstone, trap rock, river gravel, granite, and crushed sand. The investigation involved performing many standard test methods on the 26 fine aggregates. The tests performed in this study were specific gravity and absorption, flakiness, sieve analysis, sand equivalent, uncompacted void content, blue methylene, AIMS, Camsizer, mortar flow, and compressive strength of mortars.

1.1 Objectives

The main objectives of the present study are as follows:

1- To evaluate the characteristics of fine aggregate (shape, angularity, and surface texture) using indirect tests methods (the mortar flow test, the compressive strength of mortars, the uncompacted void test, and the flakiness test).

2- To evaluate the characteristics of fine aggregate (shape, angularity, and surface texture) using direct tests methods (AIMS and Camsizer).

3- To investigate the correlations between indirect and direct test methods.

4- To evaluate and compare the results of gradation analysis using the Camsizer and the sieve analysis test.

5- To investigate the micro-Deval loss for all fine aggregates.

6- To investigate the correlations between the sand equivalent test and the methylene blue test.

7- if successful, the results of this project will be used in order to see if any sands that are on the non-approved TxDOT lists would now be able to be used. In addition, based on the results of the study, modifications and suggestions will be provided for the tests.

Chapter 2: Background/ Literature Review

2.1 Need for a New Methodology

A substantial amount of research has dealt with evaluating and measuring the characteristics of fine aggregates. Many organizations have adopted different test methods, some of which are considered to be indirect tests, for evaluating and measuring the characteristics of fine aggregate. Some of these test methods, however, are not only time-consuming and prohibitively expensive, but also subject to error depending on the operator's skill. The Aggregate Image System (AIMS) can be also used to evaluate the characteristics of fine aggregates by measuring both form 2-D and angularity. The results are obtained by placing each single-sized aggregate particle on the tray and then image lightening scans and captures a certain amount of particles specified by the operator to evaluate both form 2-D and angularity. It is commonly believed that the AIMS is more accurate than conventional methods. It should be emphasized that the Camsizer system is also capable of measuring the characteristics of fine aggregates.

2.2 Literature Review

For the present study, a comprehensive literature review was conducted that primarily focused on the advances in topics related to measuring and evaluating the characteristics of fine aggregate, such as shape, angularity, and surface texture, as well as comparing and judging the results obtained using different test methods. The literature search was mainly foucsed on the following test methods: AIMS, Micro-Devol,

uncompacted void content, mortar flow test, and compressive strength of mortars. It should be pointed out that evaluating the characteristics of fine aggregates using the Camsizer was not found in the literature reviewed.

2.2.1 Topal and Sengoz, 2008

Topal and Sengoz (2008) evaluated fine aggregate angularity (FAA) using the uncompacted void test. The main objective of their study was to see whether a correlation existed between the uncompacted void content and the angularity of the fine aggregate. They collected 14 samples from different quarries and natural deposits in various areas of Turkey and conducted the uncompacted void content test on all the fine aggregates according to the uncompacted void content test, ASTM C1252. Methods A, B, and C were used to determine which method better predicted the angularity, surface texture, and sphericity of the fine aggregates. The differences between these methods are as follows: Method A specifies using a standard gradation from No. 8 to No. 100, while Method B requires performing the test on three individual fractions No. 8, No. 16, and No. 50. Method C, on the other hand, requires that the test be run on the as-received gradation. Topal and Sengoz (2008) found that Method B gave the highest uncompacted void content, which means it had the highest angularity, since the test was performed on individual size fractions. In contrast, Method C gave the lowest uncompacted void content, since this method is highly affected by the gradation of fine aggregate. Topal and Sengoz (2008) also showed that a proportional relationship existed between gradation and uncompacted void content, and that a relationship between Method B and Method C can be obtained and compared. The results obtained from both Method A and Method B

correlated well, even though Method B resulted in a higher uncompacted void content. Their recommendations were not to use Method C for predicting the angularity and shape of aggregates. They also noted that the results obtained from Method A did not predict the angularity and texture well.

2.2.2 Harini, Shaalini, and Dhinakaran, 2011

Harini, Shaalini, and Dhinakaran (2011) investigated the effect of the size and type of fine aggregates on the flowability of mortars. Their main objective was to investigate how the shape, size, texture, and type of the fine aggregate affected the flowabilty of mortar mixes. They examined two different types of fine aggregate—river and crushed sands—with four single sizes and with a single gradation for each type. They made 103 mortar mixtures with ordinary portland cement incorporating different water-cement ratios and fine aggregate-cement ratios. They used the specification for concrete aggregate, ASTM C33, and the specification for uncompacted void content, ASTM C1252, to evaluate the grain size distribution analysis and fine aggregate angularity, respectively. Their results showed that river sand had higher percentages of finer aggregates for each size compared to crushed sand. They also found that the crushed sand had a higher void content compared to river sand because irregular particles were higher for crushed sand. Their findings on this point agree with the results of other researchers. Moreover, Harini et al. (2011) found that the flowability of mortar was affected by different parameters such as aggregate type, water-cement ratio, aggregate size, and aggregate content. In regard to aggregate type, the mortar made with crushed sand had a lower spread than mortar made with river sand because, in their words,

"higher irregularities cause higher uncompacted voids resulting in demand for higher volume cement paste" (p. 166). With regard to the water-to-cement ratio, they observed that both aggregates had approximately the same trend. It is generally known that the higher the water-to-cement ratio, the higher the flowability and therefore the higher the spread. With respect to aggregate size and content, Harini et al. (2011) found that the flowability reduced as aggregate content increased. They also observed that the higher the fine aggregate-to-cement ratio, the lower the spread. According to Harini et al. (2011), "The effect of individual sizes of aggregates also plays a role in the graded mix and hence due to attention to be given on that" (p. 167).

2.2.3 Kuo and Freeman, 2007

Kuo and Freeman (2007) studied the correlation between the physical aspects of fine aggregate, such as shape, angularity, and surface texture, obtained by image-analysis testing with uncompacted void content. They examined 25 fine aggregate samples with different geometric irregularities, shape, and roundness, and surface texture; of these, 9 were natural sand aggregates and 16 were crushed aggregates. They conducted both image-analysis testing and uncompacted void contents ASTM C1252- Method B on all samples. They observed that a correlation existed between uncompacted void content and the average values of aspect ratio, angularity, and roughness, for both No. 16 and No. 30 sieve sizes. They determined the aspect ratio, angularity, and roughness using Equations 2.1, 2.2, and 2.3, respectively.

$$\text{Aspect ratio} = \frac{\text{Length}}{\text{Width}} \qquad \text{Equation 2.1}$$

$$\text{Angularity} = \left(\frac{\text{Perimeter}_{\text{convex}}}{\text{Perimeter}_{\text{ellipse}}}\right)^2 \quad \text{Equation 2.2}$$

$$\text{Angularity} = \left(\frac{\text{Perimeter}}{\text{Perimeter}_{\text{ellipse}}}\right)^2 \quad \text{Equation 2.3}$$

The coefficient of determination (R^2) for the No. 16 and No. 30 sieves was 0.91 and 0.86, respectively. Kuo and Freeman (2007) also found that aspect ratio, angularity, and roughness were linearly proportioned with the uncompacted void content. In other words, they determined that the higher the aspect ratio, angularity, and roughness, the higher the predicted uncompacted void content. Moreover, among the image analysis indices, they found that the uncompacted void content was highly influenced by particle roughness for aggregates retained on sieve No. 30, while the uncompacted void content was highly affected by the aspect ratio for aggregates retained on sieve No. 50. Kuo and Freeman (2007) concluded, "An evaluation of linear relationships among image-analysis indices revealed that roughness and angularity had the strongest correlation" (p. 64).

2.2.4 Kuo and Freeman, 2007

Kuo and Freeman (2007) studied image analysis evaluation of aggregates for asphalt concrete mixtures. Their objectives were to quantify the flatness and elongation of aggregate, to correlate the characteristics of aggregate with engineering properties of asphalt concrete mixtures, and to determine the amount of natural sand in fine aggregate. The examined eight different types of aggregate extensively, performing image analysis

testing and void content testing on all samples. They found that the image analysis test provided acceptable results compared to those of manual measurements. Kuo and Freeman (2007) said, "These manual measurements using the caliper device are tedious and rarely used on daily basis for quality control of aggregate on construction sites. However, the image analysis method is more time-efficient and provides more information" (p. 65). They also observed that image analysis techniques could account for the aspect ratio of aggregate, such as length-to-width or width-to-thickness, more accurately than the manual method of measuring flat and elongated particles of aggregate. This would allow the development of the specifications with respect to both the location and the uniformity of these distributions. In addition, Kuo and Freeman (2007) observed a linear regression of 0.91 between the image analysis indices (shape, surface texture, and angularity) and void content. They found that the image analysis technique could be used to quantify the characteristics of fine aggregate, which is an indirect way of specifying a maximum limit of natural sand. Kuo and Freeman (2007) noted that the smooth round natural sands would have an imaging index close to 1, while the manufactured sands would have smaller values. They observed that there was no clear relationship between the results of sieve analysis and an area of equivalent diameter obtained from image analysis test.

2.2.5 Al-Rousan, Masad, Myers, and Speigelman, 2006

Al-Rousan, Masad, Myers, and Speigelman (2006) developed a new methodology for classifying the shape characteristics of aggregates. The main objective of their study was to develop a thorough method for classifying aggregates based on their

characteristics, specifically those of form, angularity, and surface texture. They examined 13 coarse aggregates and 4 fine aggregates, choosing aggregates such that they covered different types of aggregates as well as different sizes and shapes. They measured form, angularity, and surface texture using AIMS. To account for variations in measurements among the operators, three operators participated in performing the tests, and each one conducted tests on two samples of each aggregate. Three different methods for comparing the results were used. The first approach was to analyze each size from all the operators separately. The second was to take the average of the No. 8 and the No. 16 samples from all the operators. According to Al-Rousan et al. (2006), "The third method was to group the analysis results obtained for each shape property from all operators and for all sizes combined" (p. 14). Figure 1 shows the results of the three different methods. They observed that the three different methods gave similar results. Al-Rousan et al. (2006) pointed out, "The group limits are similar for all sizes within the coarse and fine fractions" (p. 14). They believed that the results shown in Figure 2.1 helped develop a classification methodology, since all three methods can be used irrespective of the size of aggregate. Two terminologies, repeatability and reproducibility according to the ASTM, were used in this study to evaluate either the variations between all operators or the variation in measurements by the same operators. They also observed that repeatability and reproducibility obtained by the AIMS were very satisfactory. With respect to the effect of the size on the angularity of the fine aggregate, Al-Rousan et al. (2006) noted, "Angularity increased as particle size decreased because of crushing. The form analysis of fine aggregates showed the crushing and aggregate size had a very slight effect on the form index" (p. 17).

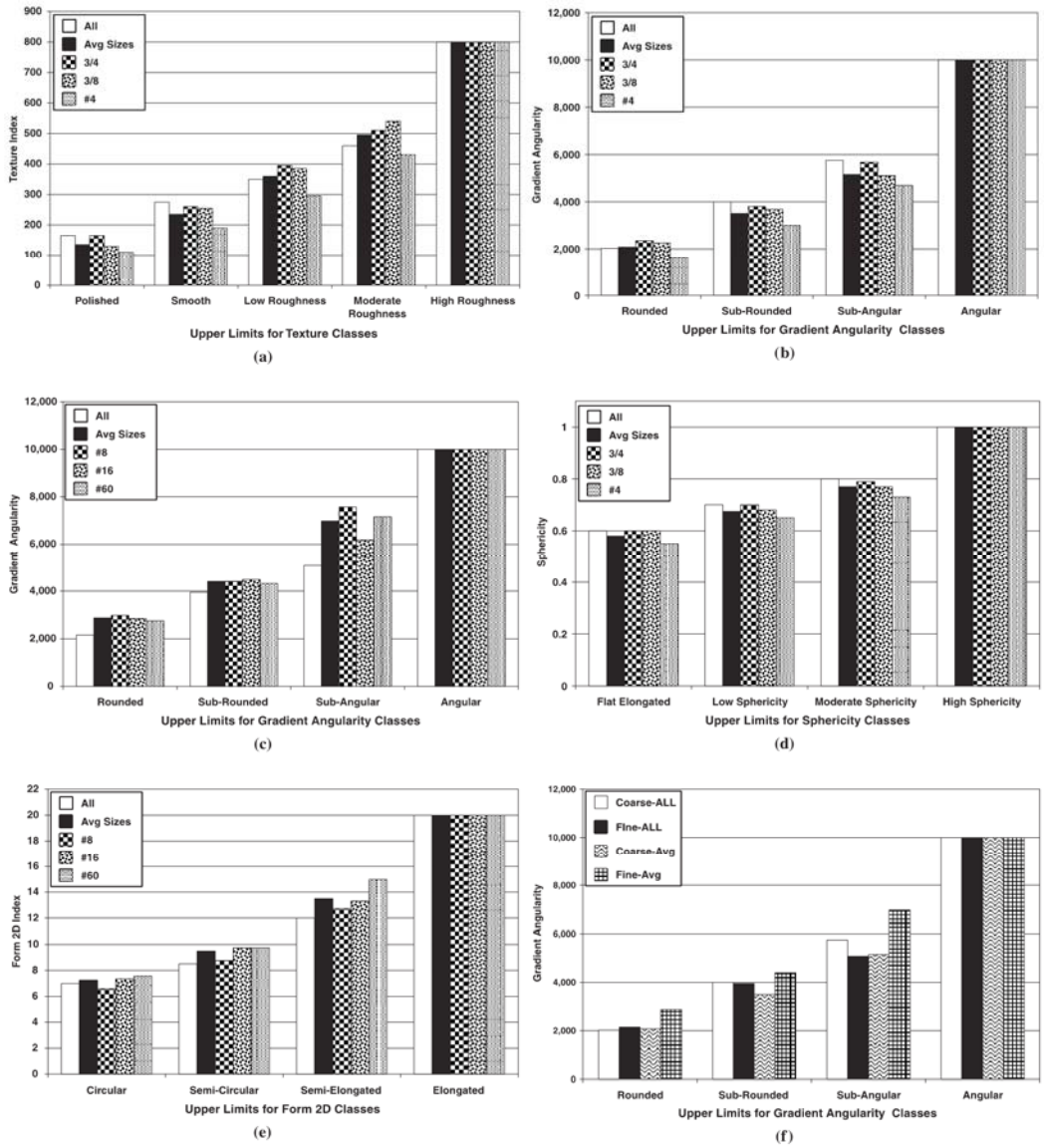

Figure 2.1: Shape Properties Groups for Individual and Combined Aggregate Sizes: (a) Coarse Aggregate Texture, (b) Coarse Aggregate Angularity, (c) Fine Aggregate Angularity, (d) Coarse Aggregate Form (Sphericity), (e) Fine Aggregate Form, and (f) Coarse and Fine Aggregate Angularity (Al-Rousan et al., 2006)

2.2.6 Mahmoud, Gates, Masad, Erdogan, and Garboczi, 2010

Mahmoud, Gates, Masad, Erdogan, and Garboczi (2010) conducted a comprehensive evaluation of the AIMS texture, angularity, and dimensional measurements. The main objective of their study was to evaluate and assess the variability, repeatability, and accuracy of the AIMS results. The aggregates were selected to cover a wide spectrum of mineralogy, including limestone, gravel, dolomite, and sandstone. They investigated the reliability of the AIMS by conducting the test on different AIMS devices, while the variability was studied by placing the aggregates on the table using four different orientations. Two methods were used to evaluate the reliability: the first involved one operator performing a test on the same samples using on two different AIMS devices; the other method involved splitting the samples into halves and having different operators test each half of the same sample using different AIMS devices. The correlation coefficient (R^2) was used to compare the results. Mahmoud et al. (2010) found that most of the results of both the before micro-Deval (BMD) and the after micro-Deval (AMD) had a value of R^2 close to 1, and observed, "The correlation of the texture results between the two AIMS units was considered acceptable" (p. 375). They evaluated the effect of the variability in the AIMS results as follows: first, the aggregates were placed randomly; second, the aggregates were rotated 90° horizontally; third, the same placement as in step 1 was used, but the aggregates were inverted so that the AIMS would scan the bottom of each particle; and finally, the aggregates were rotated 90° vertically. The results gave values of R^2 close to 1, which showed that the effect of inverting the aggregates on the AIMS results was negligible. Table 2.1 summarizes their results. Mahmoud et al. (2010) compared the accuracy of the AIMS results with X-ray CT by measuring the dimensions of aggregate particles length (L), width (W) and

thickness (T). They observed that there was an excellent correlation between the AIMS and X-ray CT: they found that the AIMS had 10% smaller values compared to the more accurate X-ray CT.

Table 2.1: Linear Modal results for Texture Analysis (Mahmoud et al., 2010)

Aggregate size	R^2 value	Best-fit linear equation	Slope CI	Intercept CI	Equality line R^2
Combined 3 sizes	0.98	U2 = 1.17 × U1 − 10.9[a]	(1.05, 1.30)	(−22.6, 0.9)	0.94
>9.5 mm	1.00	U2 = 1.09 × U1 − 4.99	(1.04, 1.14)	(−10, 0.9)	0.97
9.5–6.3 mm	0.94	U2 = 1.15 × U1 − 6.54	(0.914, 1.38)	(−28.5, 15.4)	0.88
6.3–4.75 mm	0.98	U2 = 1.25 × U1 − 15.7	(1.09, 1.41)	(−28.7, −2.7)	0.92

[a]U1 = Unit 1 and U2 = Unit 2.

Table 9. Linear Model Results for Angularity Analysis (Experiment 1)

Aggregate size	R^2 value	Best-fit linear equation	Slope CI	Intercept CI	Equality line R^2
Combined 3 sizes	0.99	U2 = 1.04 × U1 − 110[a]	(0.971, 1.11)	(−306, 86)	0.99
>9.5 mm	0.98	U2 = 1.08 × U1 − 201	(0.969, 1.19)	(−495, 94)	0.98
9.5–6.3 mm	0.98	U2 = 1.00 × U1 − 49.7	(0.892, 1.12)	(−255, 354)	0.97
6.3–4.75 mm	0.97	U2 = 1.01 × U1 − 109	(0.874, 1.16)	(−554, 336)	0.96

[a]U1 = Unit 1 and U2 = Unit 2.

Table 10. Linear Model Results for Angularity Analysis (Experiment 2)

Sample type	R^2 value	Linear equation	Slope CI	Intercept CI	Equality line R^2
BMD	0.78	U2 = 0.93 × U1 + 238[a]	(0.834, 1.03)	(−46, 522)	0.76
AMD	0.94	U2 = 1.00 × U1 − 10.4	(0.945, 1.06)	(−126, 105)	0.94
Combined	0.97	U2 = 1.03 × U1 − 59.4	(1.00, 1.05)	(−127, 8)	0.97

[a]U1 = Unit 1 and U2 = Unit 2.

Table 11. Linear Model Results for Texture Analysis (Experiment 2)

Sample type	R^2 value	Linear equation	Slope CI	Intercept CI	Equality line R^2
BMD	0.94	U2 = 0.81 × U1 + 10.5[a]	(0.76, 0.86)	(4, 17)	0.82
AMD	0.87	U2 = 0.72 × U1 + 13.6	(0.65, 0.78)	(7, 20)	0.60
Combined	0.92	U2 = 0.80 × U1 + 9.28	(0.76, 0.84)	(5, 14)	0.79

[a]U1 = Unit 1 and U2 = Unit 2.

2.2.7 Hu and Wang, 2007

Hu and Wang (2007) investigated the effect of the size and uncompacted void content of aggregate on the flowability of mortars using two types of aggregates: two river sand samples and two crushed limestone samples. They also used Type I cement was but used no chemical admixture. Five single-sized aggregates (No. 8, No. 16, No. 30, No. 50, and No. 100) and three graded aggregates, each with a different fineness modulus (FM)—3.40, 2.81 and 2.25—were extensively investigated. Hu and Wang (2007) studied

166 mortars with varying water-cement ratios (w/c) and sand-cement ratios (s/c). The tests were conducted according to ASTM specifications. They modified the flow table test to solve issues resulting from mortars with higher flowability rates before achieving 25 drops. They observed that the smaller aggregates had higher uncompacted void content, and interpreted this as meaning that larger aggregates had higher unit weights, which in turn resulted in denser packing. Among the three different fineness modules samples, they found that the uncompacted void content increased as the fineness modulus decreased. The results showed that the flowability of mortar was greatly affected by parameters such as (w/c), (s/c), and aggregate characteristics. Hu and Wang (2007) noticed that as the w/c ratio increased, the flowability of the mortar increased. This was due to the fact that an increase in the w/c ratio would result in softer paste leading to higher flowability. The effect of s/c was insignificant especially when (s/c) was the same. However, when (s/c) increased to 2 or 3, the effect was highly significant. The flowability of mortars reduced as the sand content increased. Hu and Wang (2007) attributed this reduction in the flowability of mortars to the internal friction and interlocking between solid particles. Moreover, the crushed limestone aggregates had higher uncompacted void content than those of river gravel aggregates owing to the higher angularity of the crushed limestone aggregate. Hu and Wang (2007) performed statistical analysis to develop a mathematical equation capable of determining flow in percent based on the following four parameters: w/c, uncompacted void content, sand volume and average aggregate size.

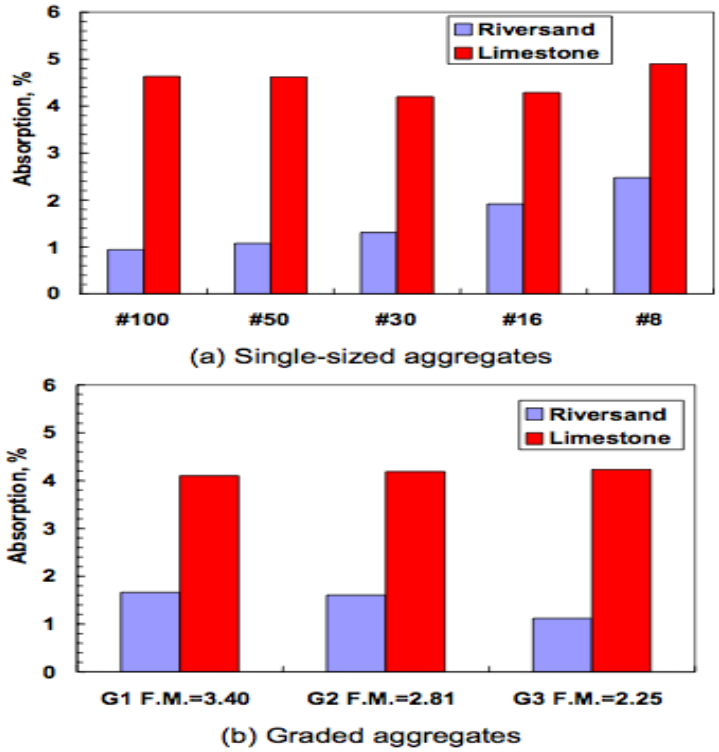

Figure 2.2: Absorption of Fine Aggregate (Hu and Wang, 2007)

2.2.8 Muszynski And Vitton, 2012

Muszynski and Vitton (2012) compared the results of fine the aggregate characteristics of roundness (R) and sphericity (S) obtained by manual/visual methods with those obtained by computer-aided methods, specifically, the automated AIMS and the NIH image program. Scales and circular templates and other drafting implements were used as manual methods. Ten fine aggregate samples were investigated and three technicians participated in the experiment. The investigated samples were selected in such a way that they all had different characteristics. The coefficient of variation (CV), the ratio of standard deviation to mean, was used to show the extent of variability. Muszynski and Vitton (2012) observed that the roundness (R) values that resulted from the manual/visual methods were lower than those of the automated methods, and the

same trend was also observed for the sphericity (S). They believed, however, that the variations in the CV values were comparable for the two methods. Figure 1 summarizes their findings. The average of the visual estimation of both R and S values carried out by the three technicians compared to the computer-aided methods was very close. According to Muszynski and Vitton (2012), "It appears that the AIMS method is able to more accurately decipher and measure 2D form/sphericity measurements; however, it should be noted that the range of sphericity of these sand specimens was not as great as for the R^2 values" (p. 204). They encouraged using automated methods since they would provide quick results when evaluating quality control of aggregates. However, they noted that some sands, such as quartz or very angular particles, were not captured and scanned by the AIMS, and they recommended that visual/ manual methods be used in this case.

Table 2.2: Roundness (R) Estimates of Particles Muszynski and Vitton (2012)

Sand name	Obs. 1 *R*	Obs. 2 *R*	Obs 3 *R*	Author estimate[a] *R*	Visual mean[c] *R*	Std. dev.[c]	CV[c](%)	"Large-scale" visual estimates[b] *R*	"Large-scale" AIMS meas.[d]
Glass beads	0.83 WR	0.80 WR	0.90 WR	0.90–1.0 WR[c]	0.87 WR	0.06	7	0.89 WR[c]	Not obtained
Ottawa sand	0.40 SR	0.40 SR	0.63 Rnd	0.55–0.60 Rnd	0.50 Rnd	0.12	24	0.48 SR	3030/6.8 SA/SR
Manistee dune	0.30 SA	0.30 SA	0.33 SA	0.35–0.40 SR	0.33 SA	0.04	11	0.34 SA	3304/7.8 SA/SA
Traverse City sand	0.28 SA	0.30 SA	0.27 SA	0.30–0.35 SA	0.29 SA	0.02	8	0.37 SR	3379/8.3 SA/SA
Gay stamp sand	0.15 VA	0.20 A	0.18 A	0.15–0.25 A	0.18 A	0.02	12	0.23 A	4058/10.8 SA/A
Crushed sand	0.20 A	0.15 VA	0.15 VA	0.10–0.20 VA	0.16 VA	0.03	20	0.18 A	3856/10.5 SA/A

[a]

2.2.9 Wang, Mohmmad, Wang and Abadie, 2005

Wang, Mohammad, Wang, and Abadie (2005) developed a unified method for quantifying aggregate shape, angularity, and texture using Fourier analysis. The main objective of their study was to determine whether Fourier analysis method was capable of quantifying the characteristics of tested aggregates, and to investigate how the results were influenced or affected when changing the orientations of particles examined. They examined 10 fine aggregate samples of known quantities with a wide range of mineralogy and used three parameters to quantify angularity, shape, and surface texture, as shown in Equations 2.1, 2.2, and 2.3. They found that to better estimate the characteristics of fine aggregates, the recommended values and terms depending on the size diameter of the particle should be used. With respect to the sensitivity of the test, Wang et al. (2005) pointed out, "This method could rank aggregate consistently with qualitative ranking based on performance and processing procedures" (p. 504). They observed that this method is statistically valid when aggregates are examined with different orientations

$$\text{shape (lumpiness)} = \sum_{m=1}^{m=n1} A_m \qquad \text{Equation 2.1}$$

$$\text{angularity (roughness)} = \sum_{m=n1+1}^{m=n2} A_m \qquad \text{Equation 2.2}$$

$$\text{surface texture} = \sum_{m=n2+1}^{m=n3} A_m \qquad \text{Equation 2.3}$$

Chapter 3: Aggregate Acquisition and Preparation

3.1 Introduction

The literature review indicated which aggregates should be included in the present study. Field performance ratings of each aggregate were requested for each source of aggregate, along with the identity of the examined sources. Providers were willing to offer aggregates with good field performance. Obtaining poor performing aggregates, however, took effort, since most providers did not want to publicize their bad aggregate sources.

A compromise was reached in which the poor quality aggregate sources would not be named in the present study in order to acquire a variety of poor-performing fine aggregates. This solution encouraged the providers to supply poor-performing aggregates without being concern that it would influence their reputation and the business of the quarry. All sources of fine aggregates were labeled for the project. Designating and labeling all sources was effective for easy reference and comparison of results.

An attempt was made to ensure there was a wide range of aggregate samples of different mineralogical backgrounds, and 26 fine aggregate sources were assembled for the present study. Table 3.1 shows the designated names of all tested fine aggregates along with their mineralogical background. The selection of fine aggregate sources of different mineralogies facilitated comparing the results and identifying which ones can be confidently used in practice and which ones are to be avoided. The following fine aggregates are classified as non-approved fine aggregates in accordance with TxDOT's specifications (ITEM 421): LS-3, LS-5, LS-8, TR-1, TR-2, and SS.

Table 3.1: The Tested Fine Aggregate Sources

Designation	Description	TxDOT status
LS-1	Limestone	Approved
LS-2	Limestone	Approved
LS-3	Limestone	Non-approved
LS-4	Limestone	Approved
LS-5	Limestone	Non-approved
LS-6	Limestone	Approved
LS-7	Limestone	Approved
LS-8	Limestone	Non-approved
LRG-1	Limestone River Gravel	Approved
LRG-2	Limestone River Gravel	Approved
LRG-3	Limestone River Gravel	Approved
LRG-4	Limestone River Gravel	Approved
LRG-5	Limestone River Gravel	Approved
RG-1	River Gravel	Approved
RG-2	River Gravel	Approved
RG-3	River Gravel	Approved
DOL-1	Dolomite	Approved
DOL-2	Dolomite	Approved
DOL-3	Dolomite	Approved
CRG-1	Crushed River Gravel	Approved
CRG-1	Crushed River Gravel	Approved
TR-1	Trap Rock	Non-approved
TR-2	Trap Rock	Non-approved
GR	Granite	Approved
SS	Sandstone	Non-approved
OS	Ottawa Sand	Approved

3.2 Aggregate Sample Preparation

3.2.1 Processing

An effective technique for preparing the delivered aggregates was required when large quantities of aggregates began arriving at the lab. The preparation process involved sieving, washing, drying, and bagging, and it took a substantial amount of time to complete. Generally, sieving was the first action. Each source of the 25 fine aggregates was passed through a group of sieves having different standard sizes as follows: 4.75 mm (No. 4), 2.36 mm (No. 8), 1.18 mm (No. 16), 600 μm (No. 30), 300 μm (No. 50), 150 μm (No. 100), and 75 μm (No. 200). A five-gallon bucket was used to separate each size fraction.

After separating the fine aggregates into different size fractions and making sure the fine aggregates were clean and free of any deleterious particles, the samples were placed into an oven at a temperature of 110 ± 5°C (230 ± 9°F) for one day. The samples were then taken out of the oven and then allowed to cool for about 2 to 3 hours. Then, each sample was replaced into a bucket. In order to prevent the samples from absorbing moisture and to ensure the test samples remain in oven-dry condition, the buckets were sealed and stored inside.

Bagging and labeling the aggregate samples facilitated the process of performing tests. Bagging basically involved weighing out the fine aggregates into suggested masses for each test procedure, labeling each bag, performing tests, and storing the samples until they were ready for testing. The bagging process was found to be a very effective method of preparing and dealing with a large quantity of fine aggregate samples for testing. As most of the tests were conducted at locations other than the main laboratory, selecting,

transporting, and testing of the samples was straightforward. Extra fine aggregates were kept in the buckets for future testing if needed.

3.3 Performing Test Procedures

The fine aggregate samples were ready for testing as soon as the bagging process was completed. Testing was conducted in a manner that was as similar as possible to the applicable specifications. Additional effort was put into achieving consistent results from testing batch to batch, as well as having the same person conduct the test on all samples. This was done in order to eliminate or at least to reduce the variability when more than one person conducts a specific test.

Chapter 4: Experimental Methods and Procedures

4.1 Introduction

This chapter describes all the experimental test methods used in this study. The description of these test methods includes presenting the objective of each test and the procedures followed. Specific gravity and absorption, sand equivalent, blue methylene, the AIMS, the Camsizer, flakiness, sieve analysis, uncompacted void content, the flow table, and the compressive strength of mortars are explained in detail.

4.1 Specific Gravity and Absorption Test

The ASTM C 128 "Standard Method of Test for Specific Gravity and Absorption of Fine Aggregate" was used to evaluate the bulk and apparent specific gravity and the absorption capacity of fine aggregate at a stated temperature of 23° C (73.4°F).

Bulk specific gravity is one of the important physical properties used to provide information about the volume taken up by the aggregate in different mixtures such as portland cement concrete and bituminous concrete. Bulk specific gravity can also be used to estimate the voids in aggregate. The bulk specific gravity is determined either on a saturated surface-dry basis or an oven-dry basis, depending on the moisture condition of aggregate.

The ASTM (2007) defines the apparent specific gravity as "the ratio of the weight in air of a unit volume of the impermeable portion of aggregate at stated temperature to the weight in air of an equal volume of gas-free distilled water at a stated temperature." The apparent specific gravity is rarely used in construction aggregate technology.

Absorption is defined as the increase in the mass of aggregate because of water absorbed in the pores of the materials, not including water on the outside surface of the particles, compared to the dry condition. The absorption is determined by submerging a dry sample of aggregate in water for roughly 15 hours.

4.1.1 Preparation of Test Specimen

A fine aggregate sample of one kilogram was obtained. The sample was then dried in a suitable pan at a temperature of 110 ± 5°C (230 ± 9°F). The sample was allowed to cool to an acceptable temperature, and then was immersed in water. The sample was allowed to stand for 15 to 19 hours. Additional water was poured in without losing any fine aggregate. The sample was spread on a flat surface and exposed to a soft current of warm air and stirred regularly to achieve homogenous drying. After the material began to dry, it was very important to work it either by hand or by other means to prevent the sample from being conglomerated or held together. This process was maintained until the sample reached a free-flowing condition. Figure 4.1 shows the standard apparatus used for this test method.

4.1.2 Procedure

After partly filling the pycnometer with water, a 500-g saturated surface-dry fine aggregate specimen was placed into the pycnometer. Additional water was added to the pycnometer until it reached nearly 90% of its capacity. The air bubbles in the pycnometer were eliminated physically by rolling and agitating the pycnometer or mechanically by vibrating the pycnometer. The temperature was maintained at 23 ± 1.7°C (73.4 ± 3°F).

The total mass of the pycnometer, specimen, and water was determined. The fine aggregate specimen was removed from the pycnometer and put in an oven at a temperature of 110 ± 5°C (230 ± 9°F) to dry out for one day. The fine aggregate was allowed to cool by exposing it to air at a room temperature for approximately one hour. The mass of the fine aggregate sample was then determined.

Bulk specific gravity is calculated using Equation 4.1.

$$\text{Bulk specific gravity} = \frac{A}{B + S - C} \qquad \text{Equation 4.1}$$

Apparent specific gravity is calculated using equation 4.2.

$$\text{Apparent specific gravity} = \frac{A}{B + A - C} \qquad \text{Equation 4.2}$$

Absorption is determined using equation 4.3.

$$\text{Absorption} = \left(\frac{S - A}{A}\right) \text{X } 100 \qquad \text{Equation 4.3}$$

where

A = mass of oven-dry specimen in air, g;

B = mass of pycnometer filled with water, g;

S = mass of saturated surface-dry specimen, g; and

C = mass of pycnometer with specimen and water to calibration mark, g.

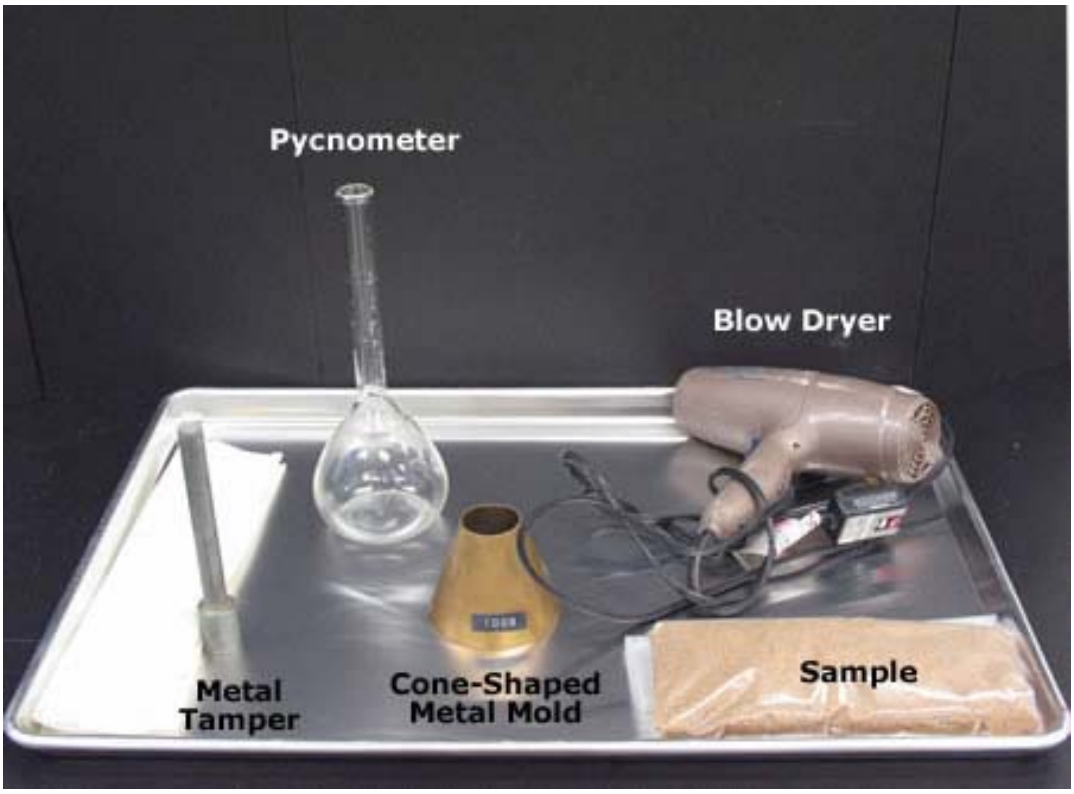

Figure 4.1: Standard Apparatus Used for Measuring Specific Gravity and Absorption of Fine Aggregate

4.2 Sand Equivalent Test

The ASTM D 2419 "Standard Test Method for Sand Equivalent Value of Soils and Fine Aggregate" was performed to evaluate the relative amount of harmful fine dust or clay-like particles in soils and fine aggregates. According to Lay (2009), "The original form was developed by Hveem of California Division of Highway in 1953. However, the common current version is based largely on a French variant." The sand equivalent is defined as the ratio of sediment height to the flocculent height in the plastic cylinder.

4.2.1 Preparation of Test Specimen

A representative sample of material satisfying the adopted specifications was chosen. The selected sample was oven dried to a constant weight at a temperature of 110 ± 5°C (230 ± 9°F). After removing the test sample from the oven, the sample was allowed to cool down to room temperature. The 4.75 mm (No. 4) sieve was used to separate the sample into two different portions such that one portion had particles passing the 4.75 mm (No. 4) sieve and the other had particles retained on the 4.75 mm (No. 4) sieve. A 500-g sample was obtained from the portion passing the 4.75 mm (No. 4) sieve. The sample was split into three sizes: passing the 4.75 mm (No. 4), retained on the 2.36 mm (No. 8) sieve, and passing the 2.36 mm (No. 8) sieve. The three sizes were mixed in a proper quantity in order to obtain a representative uniform sample. The test sample was put in the measuring can and excess material was removed using a spatula. Figure 4.2 shows the standard apparatus used for this test method.

4.2.2 Procedure

The quantity of flocculating calcium chloride was poured into the plastic cylinder. The sample was then transferred from the measuring can into the plastic cylinder using a funnel. After stoppering the cylinder, the cylinder was agitated and tapped to remove air bubbles and promote wetting the sample. After a specific sedimentation period, the height of the sand as well as the height of the clay were determined. The sand equivalent value was determined by Equation 4.4.

$$\text{Sand Equivallent Value (SE)} = \left(\frac{\text{Sand Reading}}{\text{Clay Reading}}\right) \text{X } 100 \qquad \text{Equation 4.4}$$

where

Sand reading = height of sand in cylinder (mm); and

Clay reading = height of clay in cylinder (mm)

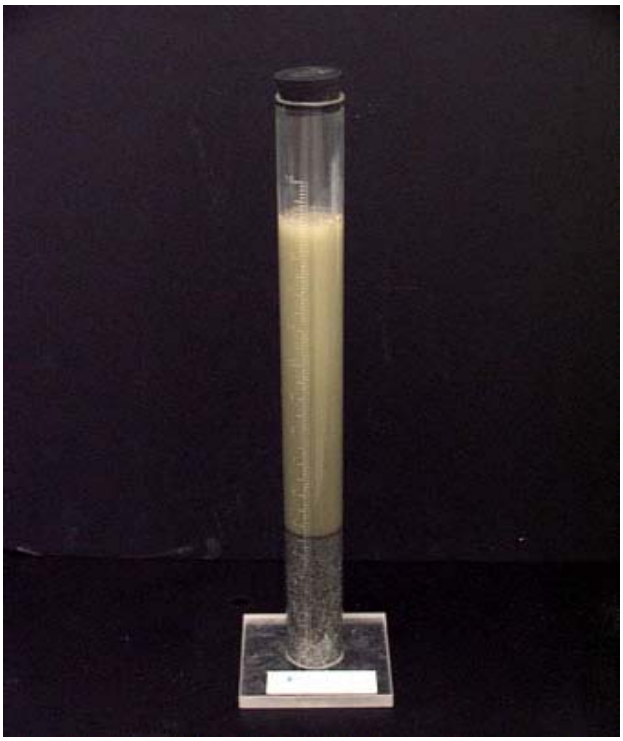

Figure 4.2: Apparatus Used for Measuring Sand Equivalent of Fine Aggregate

4.3 Methylene Blue Test

The ASTM C 837 "Standard Test Method for Methylene Blue Index of Clay" was used to recognize the presence of harmful clays of the smectics group (poor minus 75 μm (No. 200)) and to give a sign of the surface activity of the aggregates. The amount of the methylene blue solution added to the sample can be used to predict the amount of harmful clays and organic materials in aggregate. A higher amount of the methylene blue

value signifies a higher amount of clay or organic material in the sample. Table 4.1 shows the expected performance of methylene blue.

Table 4.1: The Expected Performance of Methylene Blue (ASTM C 837, 2009)

Methylene Blue (mg/g)	Expected performance
≤ 6	Excellent
7-12	Marginally acceptable
13-19	Problems/possible failures
≥ 20	Failure

4.3.1 Procedure

The test was conducted on a washed and dry sample passing the 75-μm (No. 200) sieve. A sample of 10 g of the material passing the 75-μm (No. 200) sieve was placed in a 500-ml griffin beaker. Slurry was made by adding 30 ml of distilled water and mixing it with a mixer. The burette, a glass tube with measurements on it, was filled with the methylene blue solution. The ASTM C 837 requires starting with 0.5 ml of the solution and stirring for approximately 1 min. The drop of the slurry was removed using the glass-stirring rod and a filter paper was placed on. The appearance of the drop on the filter paper was observed, and the solution of methylene blue was continually added to the slurry in an incremental way such that 0.5 ml was added and then was stirred for 1 min each time until the end of the point was reached. Stirring was continued for 5 minutes. Once the end point was reached, the measurement was recorded. The methylene blue

value was determined using Equation 4.5. Figure 4.3 shows the standard apparatus used for this test method.

$$M = \frac{C\,V}{W} \qquad \text{Equation 4.5}$$

where

C = mg of methylene blue/mL of solution;

V = mL of methylene blue solution required for titration; and

W = grams of dry material

Figure 4.3: Apparatus Used for Measuring Blue Methylene

4.4 Sieve Analysis Test

The ASTM C 136 "Standard Test Method for Sieve Analysis of Fine and Coarse Aggregates" was performed to determine the particle size distribution of fine aggregate with applicable specification requirements by sieving. This test could also be beneficial in establishing a relationship between porosity and packing.

4.4.1 Procedure

A 500-g test sample was prepared. The test sample of fine aggregate was oven dried. Sieves with appropriate openings, as shown in Figure 4.4, were selected according to the ASTM C 136. The nominal maximum size square openings used in this test are illustrated in Table 4.2. The sieves were agitated by mechanical devices for a satisfactory period of time (approximately 10 minutes). The mass of fine aggregate retained on each sieve was recorded. The percentage of the mass retained on each sieve was then calculated.

Table 4.2: The Nominal Maximum Size Square Openings Used

Nominal maximum size square openings mm (in)
4.75 mm (No. 4)
2.36 mm (No. 8)
1.18 mm (No. 16)
600 µm (No. 30)
300 µm (No. 50)
150 µm (No. 100)
75 µm (No. 200)
Pan

Figure 4.4: Apparatus Used for Sieve Analysis Test

4.5 Uncompacted Void Content of Fine Aggregate

The ASTM C 1252 "Standard Test Methods for Uncompacted Void Content of Fine Aggregate" was performed to determine the void content of fine aggregate, which provides more information about the characteristics of fine aggregate (angularity, sphericity, and surface texture). There are three different methods of measuring the void content of fine aggregate, Methods A, B, and C.

Method A is called the standard graded sample. In this method, a standard fine aggregate grading is achieved by mixing individual sieve fractions from the sieve analysis test of fine aggregate used. The required amount of each individual size fraction is shown in Table 4.3. Method A is considered the most suitable as a quick test that can give information about the particle shape characteristics of a graded fine aggregate sample. It is useful because the materials used in this method can be acquired from the remaining size fraction after the single sieve analysis test of the fine aggregate is conducted.

Method B is called individual size fractions. In the present study, three different size fractions were used: a) 2.36 mm (No. 8) to 1.18 mm (No. 16); (b) 1.18 mm (No. 16) to 600 μm (No. 30); and (c) 600 μm (No. 30) to 300 μm (No. 50); each of these are tested separately. Method B is more time-consuming since each size fraction has to be tested separately and it requires a larger amount of a sample than other methods. However, more information about the shape and texture characteristics of each individual size fraction is obtained.

Method C is called received grading. The only requirement for this method is that the tested aggregate be finer than a 4.75mm (No. 4) sieve. Method C may be suitable in determining the proportions and components used in mixtures.

Table 4.3: The Required Amount of Each Individual Size Fraction (ASTM C 1252, 2006)

Individual Size Fraction	Mass, g
2.36 mm (No. 8) to 1.18 mm (No. 16)	44
1.18 mm (No. 16) to 600 μm (No. 30)	57
600 μm (No. 30) to 300 μm (No. 50)	72
300 μm (No. 50) to 150 μm (No. 100)	17

4.5.1 Procedure

A 190-g fine aggregate sample was poured into a funnel of a fixed height after blocking the opening of the funnel by a finger. The sample in the funnel was kept level using the spatula. The sample was allowed to fall freely into the cylindrical measure by removing the finger. All excess fine aggregate from the cylindrical measure was removed by a quick pass of the spatula. The ASTM C 1252 requires that the cylindrical measure not be vibrated, since that provides extra compaction, which affects the results. The uncompacted void content was determined using Equation 4.6.

$$U = \frac{V - (F/G)}{V} \text{ X } 100 \qquad \text{Equation 4.6}$$

where

V= volume of cylindrical measure, mL;

F= net mass, g, of fine aggregate in measure (gross mass minus the mass of the empty measure);

G= bulk dry specific gravity of fine aggregate; and

U= uncompacted voids, percent, in the material.

Figure 4.5: Apparatus Used for measuring Uncompacted Void Content

4.6 Flakiness Test of Fine Aggregate

The Materials Engineering and Research Office, MERO-034 "A Flakiness Test for Fine Aggregate" was used to determine the amount of flaky particles in fine aggregate. The amount of flaky particles can provide valuable information on how fine aggregate contributes to ease of compaction in a dense graded mixture. The flakiness test was conducted on both 2.36 mm (No. 8) and 1.18 mm (No. 16) sieves. Lower water demand in hydraulic cement concrete can result from material of low flaky particles. The type of crusher and the reduction area influence the amount of flaky particles. Figure 4.7 shows the standard apparatus used for this test method.

4.6.1 Procedure

A 50-g sample was obtained from each size fraction (both 2.36 mm (No. 8) and 1.18 mm (No. 16) sieves). The sample was washed and then oven dried. The entire sample was placed on the slotted sieve and was sieved manually. Care was taken not to lose any material by using a close-fitting cover and a pan. The mass of particles retained on the flakiness sieve after sufficient sieving was determined. The flakiness particles for each fraction were evaluated using Equation 4.7. Figure 4.6 shows the standard apparatus used for this test method.

$$\text{Flakiness } (\%) = \left(\frac{A - B}{A}\right) \text{X } 100 \qquad \text{Equation 4.7}$$

where

A= the original mass of a material; and

B= the mass of a material retained on a slotted sieve

Figure 4.6: Apparatus Used for Flakiness Test of Fine Aggregate (MERO-034, 2009)

4.7 Aggregate Image System (AIMS)

The AASHTO TP 81 "Standard Method of Test for Determining Aggregate Shape Properties by Means of Digital Image Analysis" was performed to determine the shape characteristics of aggregate. Two main characteristics are evaluated and determined for fine aggregates in this test: form 2-D and gradient angularity. Figure 4.7 illustrates the way the form 2-D and gradient angularities are measured.

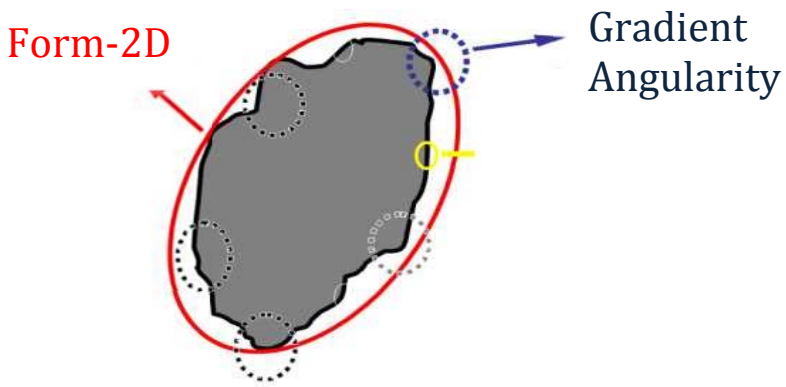

Figure 4.7: Form 2-D and Gradient Angularity of Fine Aggregate particle

The relative form of two-dimensional images of fine aggregate particles is evaluated and quantified by analyzing the black-and-white image of a particle projection. The form 2-D has a domain of 0 to 20. A zero value of form 2-D means a perfect circle. The form 2-D is determined using Equation 4.8.

$$\text{Form } 2-\text{D} = \sum_{\theta=0}^{\theta=360-\Delta\theta} \left[\frac{R_{\theta-\Delta\theta} - R_{\theta}}{R_{\theta}}\right] \qquad \text{Equation 4.8}$$

where

R_θ = the radius of the particle at angle θ; and

$\Delta\theta$ = the incremental difference in the angle.

The gradient angularity is another important feature used to evaluate and determine how sharp the corners of two-dimentional images of fine aggregate particles are. The higher gradient value, the more angular the shape is. The angularity falls in the range of 0 to 10,000 with a zero value indicating a perfect circle. The angularity is determined using Equation 4.9.

$$\text{Angularity} = \frac{1}{\frac{n}{3}-1}\sum_{i=1}^{n-3}[\theta_i - \theta_{i+3}] \qquad \text{Equation 4.9}$$

where

θ = the angle of orientation of the edge points;

n = the total number of points; and

I = denoting i^{th} point of the edge of the particle.

4.7.1 Procedure

The AIMS setting was adjusted so that each size fraction of retained material was analyzed separately. The fine aggregate samples were distributed over the black tray in such a way that the particles were separated from each other. The analysis was run by digital image acquisition sequence. Once the size fraction was selected, the AIMS device captured the required images to determine the characteristics of each particle. A minimum number of fine aggregate particles (150 particles) was chosen to evaluate and measure in to order to provide reliable results.

Figure 4.8: The AIMS Device

4.8 Dynamic Image Analysis System (Camsizer)

The Camsizer evaluates the shape characteristics of fine aggregates as well as the particle size distribution with applicable specification requirements. Four important

parameters are obtained from the Camsizer: elongation, convexity, sphericity, and symmetry.

The elongation is defined as the ratio of the width of a particle to its length. Equation 4.10 is used to calculate the elongation. Circular particles have a ratio of 1. Elongation is illustrated in Figure 4.8.

$$\text{Elongation} = \frac{X_{C\,min}}{X_{Fe\,max}} \quad \text{Equation 4.10}$$

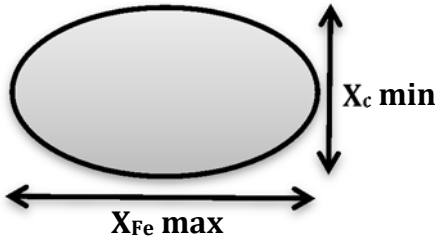

Figure 4.9: Elongation Measurement of a Fine Aggregate Particle

The convexity is defined as the ratio of the actual area of a fine aggregate particle to the area of the convex shell. The convexity criterion provides information about how smooth or rough the surface is. Generally, a convexity value of 1 is obtained for a smooth surface, whereas a lower value is expected for a rough surface. Equation 4.11 is used to determine the convexity. Figure 4.11 illustrates how the area of the convex shell is calculated.

$$\text{Convexity} = \sqrt{\frac{A_{real}}{A_{convex}}} \quad \text{Equation 4.11}$$

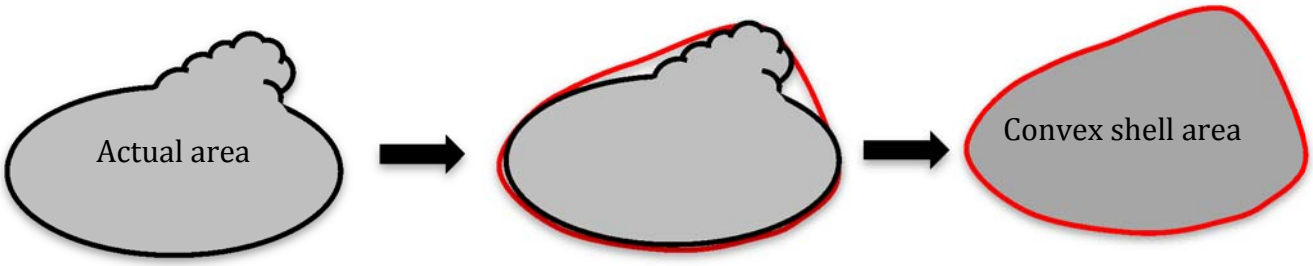

Figure 4.10: Diagram Showing How Convex Shell Area Is Determined

The sphericity or (roundness) is also described as the ratio of the area of a fine aggregate particle to its perimeter. Circular particles or angular particles have a sphericity (roundness) value of 1, while a lower value is expected for irregular particles. Equation 4.12 is used to determine sphericity or roundness.

$$\text{Sphericity} = \frac{4\pi A}{P^2} \quad \text{Equation 4.12}$$

The symmetry is determined by first finding the center of the particle C. Then, many lines are drawn in such a way that each line passes through the center of the particle. From these lines passing through the center, the minimum ratio of the bigger to the smaller radius (r_1/r_2) is then computed, as shown in Figure 4.11. The symmetry is determined by using Equation 4.13. Circular particles have a symmetry value of 1, while elliptical particles have a symmetry value of near 1. The importance of the symmetry parameter is its ability to identify broken particles within a sample.

$$\text{Symmetry} = \frac{1}{2}\left(1 + \min\left(\frac{r_1}{r_2}\right)\right) \quad \text{Equation 4.13}$$

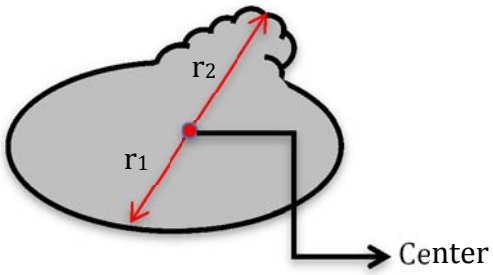

Figure 4.11: Diagram Showing How Symmetry Is Measured

4.9 Micro-Deval Test

The ASTM D 7428 "Standard Test Method for Resistance of Fine Aggregate to Degradation by Abrasion in the Micro-Deval Apparatus" was performed to determine the resistance of fine aggregates to abrasion in the presence of water and an abrasive charge. The ASTM D 7428 requires that Micro-Deval be conducted on a wet sample since many fine aggregates are more vulnerable to abrasion when wet than dry. The Micro-Deval test of fine aggregate provides valuable information on assessing the toughness/abrasion resistance of fine aggregate as well as measuring the quantity of soft and weak material in fine aggregates such as shale and shaley carbonate. The ASTM D 7428 showed that a relationship between the drying shrinkage of cement mortars and Micro-Deval exists. The Micro-Deval machine is shown in Figure 4.12.

4.9.1 Procedure

A 500-g sample was obtained and prepared. The sample then was immersed in 0.75 ± 0.05 L of tap water at a temperature of 20 ± 5°C for one hour. Then 1250-g steel balls were added to the prepared test sample. The Micro-Deval container was covered and placed on the machine. The machine was run at 1500 revolutions per minute for 15 minutes. The sample and steel balls were then poured on a 6.3 sieve into a suitable container to avoid losing the fine aggregate sample. The fine aggregate was washed after the steel balls were removed and was then dried in an oven at a temperature of 100 °C. The mass of the sample was then recorded. The Micro-Deval abrasion loss was determined using Equation 14.

$$\text{Percent Loss} = \frac{(A-B)}{A} X100 \quad Equation\ 14$$

where

A = the original mass of the test sample; and

B = the mass of the test sample after conducting micro-Deval.

Figure 4.12: Apparatus Used for Micro-Deval of Fine Aggregate

4.10 Compressive Strength of Hydraulic Cement Mortars

The ASTM C109/C109M "Standard Test Method for Compressive Strength of Hydraulic Cement Mortars (Using 2-in. or [50-mm] Cube Specimens)" was performed to determine the compressive strength of hydraulic cement mortars using standard 2-in or 50-mm cube specimens. According to ASTM C109/C109M, the ratio of sand to cement used for making the mortars is specified and portioned by mass as follows (sand: cement = 1:2.75). In addition, the amount of water cement ratio used in producing the mortars mainly depends on portland cement characteristics. Therefore, water-cement ratio of 0.485 is used for all portland cements. However, a lower water-cement ratio is used for all air-entraining cements.

The mixture proportions used for making mortars are illustrated in Table 4.4. The grading requirements for fine aggregate used for making mortars are shown in Table 4.5.

Table 4.4: The Mixture Proportions of Mortars

Cement, g	500
Sand, g	1375
Water, ml	242
Water-cement ratio	0.485

Table 4.5: The Grading Requirements for Fine Aggregate

	%Passing	%Retained
#4	100	0
#8	77	23
#16	54	23
#30	30	24
#50	14	16
#100	0	14

4.10.1 Procedure for Mixing Mortars

The mixing water was placed in the bowl. The cement was added to the water after the dry paddle and the dry bowl were put in the mixing position in the mixture. The mixer was turned on to mix the mixing water and cement for 30 seconds at the minimum speed. The entire amount of sand was slowly added over a 30-second period while the mixer was running at low speed. The mixer was stopped just long enough to change the mixing speed to medium speed and then was run for 30 seconds. The mixer was again stopped for 90 seconds. An effort was made to scrape down any mortar that had gotten stuck on the bowl's sides. The mixer was then turned on at medium speed for 60 seconds. The specimens were prepared and the mortar was placed into the cubes in two layers such that each layer was filled approximately 1 in (25 mm). The mortar was tamped in each cube 32 times in four rounds within 10 seconds. Figure 4.13 shows the standard method of tamping the cube specimens. The excess mortar on the surface was removed to obtain a level surface. After completion of molding, the cube specimens were placed in the moist room for 20 to 72 hours without exposing the surface to dripping water.

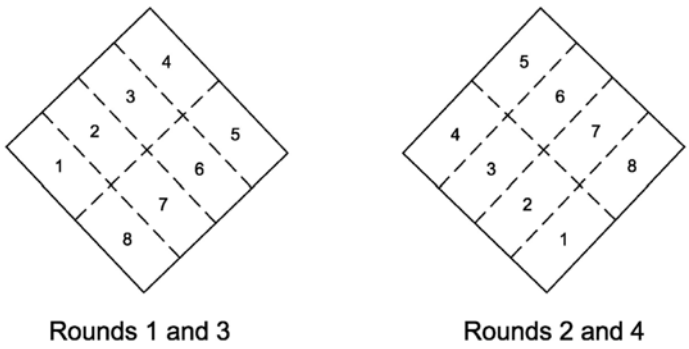

Figure 4.13: Order of Tamping in Molding of Test Specimens

Figure 4.14: Apparatus used for making mortars

4.11 Mortar Flow Test

The ASTM C 1437 “Standard Test Method for Flow of Hydraulic Cement Mortar” was performed to determine the flow table of hydraulic cement mortars.

4.12.1 Procedure

The flow mold was placed at the center of the flow table, as shown in Figure 4.15. The flow table was kept clean and dry. A layer of mortar was placed in the mold such that half of the flow mold was filled with the mortar. The mortar was tamped uniformly and sufficiently 20 times using a tamper. The other half was filled with the mortar and was tamped in the same way as the first layer. The excess mortar was removed to obtain a level plane surface. After lifting the flow mold away from the mortar, the table was rapidly dropped 25 times within 15 seconds. The diameter of the mortar from four different specified lines was measured. The total flow in percent was determined as the sum of those four readings.

Figure 4.15: Apparatus Used for Mortar Flow Test

4.13.1 Procedure for Determining the Compressive Strength of Mortars

With a large number of mortar cubes, the test specimens were kept immersed in a bucket filled with water at a temperature of 23 ± 1.7°C (73.4 ± 3°F) after removal from

the curing room. The surfaces of the specimens were prepared to remove any loose sand grains in order to achieve a surface-dry condition. The testing machine was turned on and the setting was adjusted. The test specimen was placed appropriately in the center and the load was applied. The load rate was maintained within the allowable range (200 to 400 1bs/s [900 to 1900 N/s]). The maximum load was recorded and the compressive strength of the mortars was determined using Equation 4.15.

$$\text{Compressive strength (fm)} = \frac{P}{A} \qquad \text{Equation 4.15}$$

where

fm =compressive strength in psi or [MPa];

P = total maximum load in lbf or [N]; and

A = area of loaded surface in2 or [mm2].

Chapter 5: Results and Discussion

5.1 Introduction

This chapter presents the results of all tests performed. An analysis consists of evaluating the result of each test based on mineralogy, finding the correlations between test methods, and comparing the results of the approved fine aggregates with the non-approved ones.

5.2 Uncompacted Void Test Results

The uncompacted void content test (ASTM C 1252) discussed in section 4.5 was performed on the 26 fine aggregates to evaluate the shape, texture, and angularity by comparing the packing densities. The uncompacted void content was determined according to the following methods: Method A, standard graded sample; Method B, individual size fraction; and Method C, as-received grading.

The results of the uncompacted void test using Methods A, B, and C are shown in Figure 5.1. Method B had the highest percentage of uncompacted void, while Method C had the lowest percentage of uncompacted void. The limestone, dolomite, and trap rock fine aggregates had the highest percentage of uncompacted void, whereas the river gravel and limestone river gravel sands had the lowest. It should be noted that an increase in void content indicates higher angularity, less sphericity, and rougher surface texture. Conversely, a decrease in void content indicates a rounded, smooth, and spherical surface.

Method A was found to be the most effective method since the sample used in this method can be obtained from the remaining size fractions after performing sieve analysis on each sieve of fine aggregate. Method B is time-consuming because the test method has to be conducted on each size fraction, which means a larger sample is required; however, this method provides more information about the shape and texture of each size fraction.

Method C failed to evaluate the characteristics of the fine aggregate and didn't follow the trends observed for both Methods A and B. This is attributed to the fact that Method C uses that portion of the fine aggregate finer than a 4.75-mm (No. 4) sieve unlike with other Methods A and B.

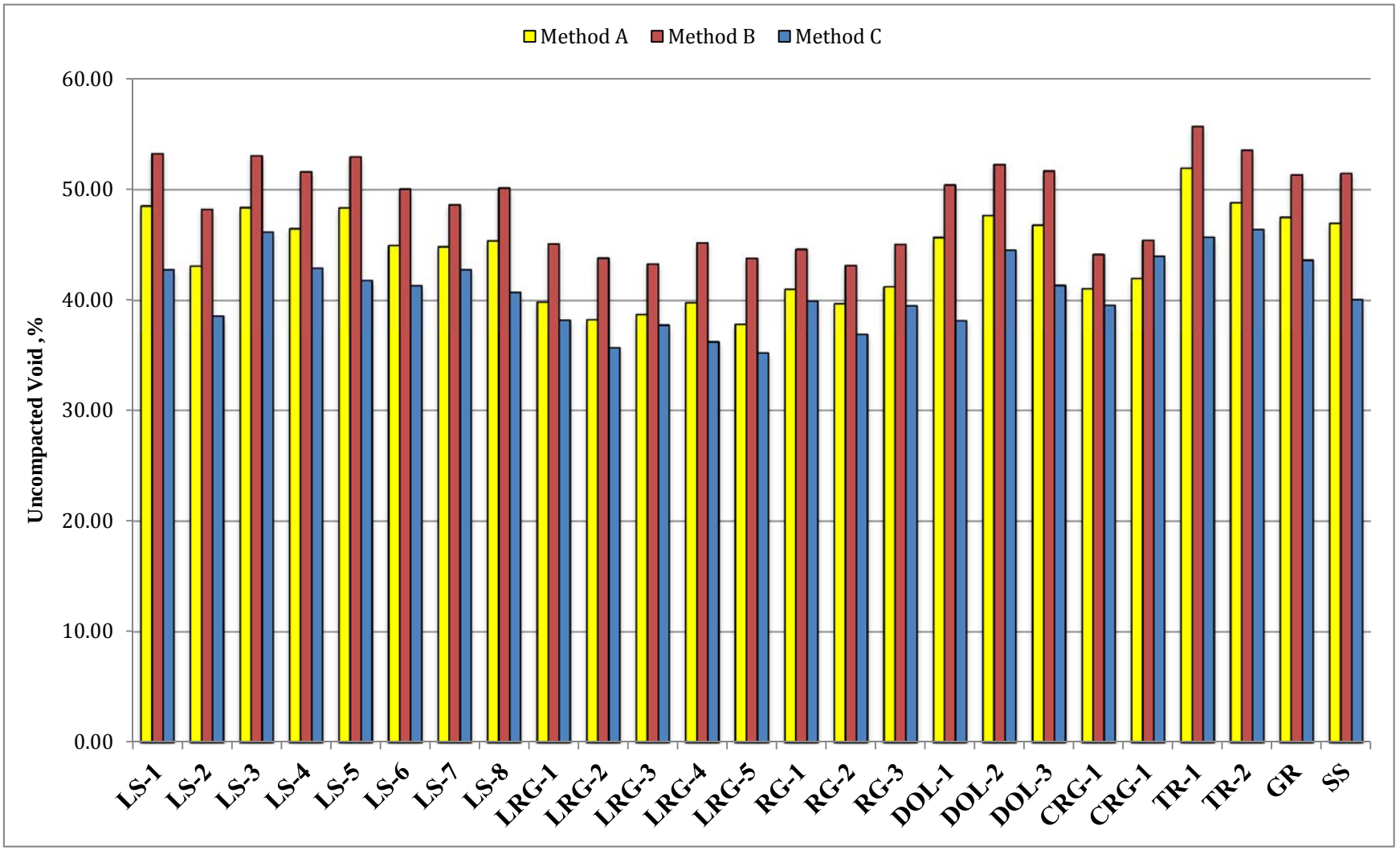

Figure 5.1: Uncompacted Void Test Results

Table 5.1: Uncompacted Void Test Results Based on Mineralogy

Fine aggregate type	Method A	Method B	Method C
Limestone	46.25	50.99	42.13
Limestone River Gravel	38.89	44.24	36.60
River Gravel	40.64	44.28	38.76
Dolomite	46.71	51.46	41.35
Crushed River Gravel	41.52	44.78	41.77
Granite	47.49	51.35	43.63
Sandstone	46.95	51.46	40.08

5.3 Mortar Flow Test Results

The mortar flow test (ASTM C 1437) discussed in section 4.11 was performed on the 26 fine aggregates to evaluate the shape, texture, and angularity by comparing workability. The ASTM C 1437 was conducted both on the as-received sands and on the regraded sands. The mixture design for the mortar was based on a water-cement ratio (w/c) of 0.485 and a sand-cement ratio (s/c) of 2.75. The volumetric proportions for the mortar mixture are shown in Table 5.2; the grading requirement for making the mortars was chosen to meet ASTM C33, as shown in Table 5.3.

Table 5.2: The Mixture Proportions of Mortars

Cement, g	500
Sand, g	1375
Water, ml	242
Water-cement ratio	0.485

Table 5.3: The Grading Requirements for Fine Aggregate

Sieve	%Passing	%Retained
No.4	100	0
No.8	77	23
No.16	54	23
No.30	30	24
No.50	14	16
No.100	0	14

The results of the mortar flow test performed both on the as-received sands and on the regraded sands are shown in Figure 5.3. The regraded sands generally had a higher percentage of flow compared to the as-received sands. The flow in percent was determined by measuring the diameter of the mortar along the four lines marked on the tabletop; the diameter of the tabletop itself was 40 in.

The average values of flow in percent based on the mineralogy of the fine aggregates are shown in Figure 5.2. The river gravel and limestone river gravel sands had the highest percentage of flow both for the as-received sands and for regraded sands. However, the limestone and sandstone sands had the lowest percentage of the flow both for both categories. Thus, it can be said that the rounded, spherical and smooth surfaces of the fine aggregates tend to have higher flow, whereas lower flow indicates higher angularity, less sphericity and rougher surface texture.

The variations in the percentage of flow between the as-received and the regraded sands varied from 2 to 15%, as shown in Table 5.4. However, the difference was very

large for the trap rock sand, because the trap rock fine aggregates had the highest average void content among all the fine aggregates.

Table 5.4: Mortar Flow Test Results Based on Mineralogy

Fine aggregate type	% As-received sand	% Regraded sand	% Difference
Limestone	91	100	11
Limestone River Gravel	139	156	13
River Gravel	140	160	14
Dolomite	128	138	8
Crushed River Gravel	129	145	13
Trap Rock	85	138	63
Granite	113	130	15
Sandstone	86	84	2

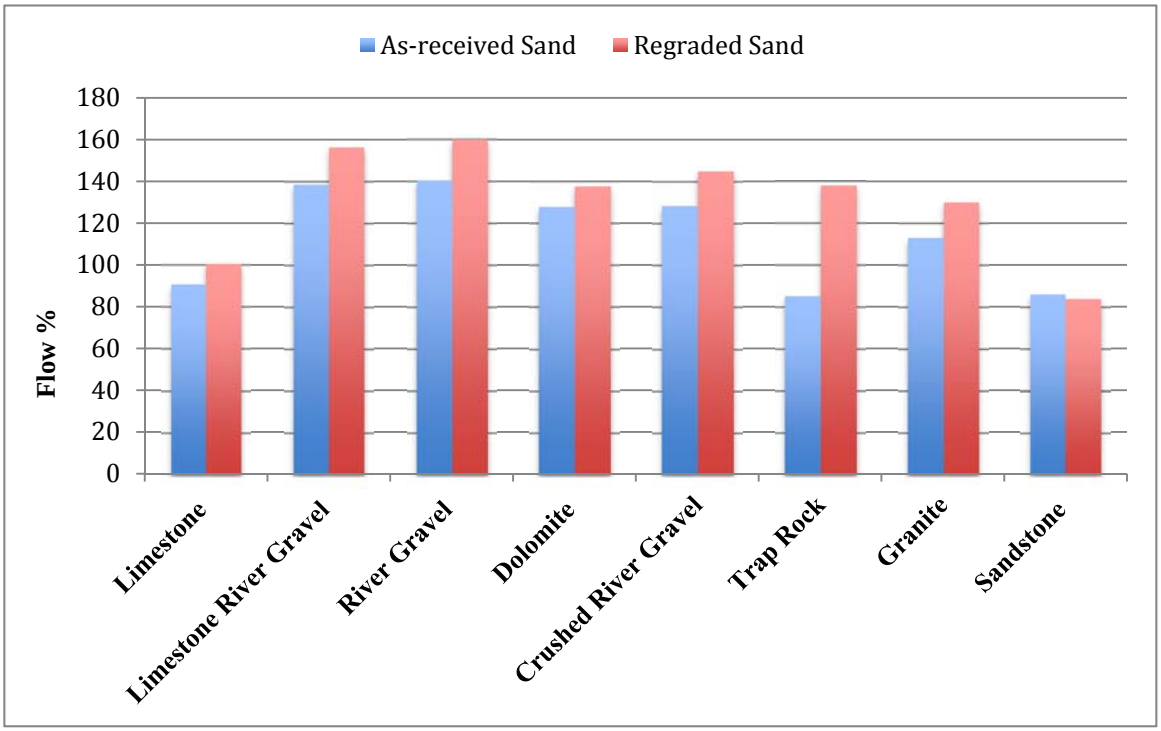

Figure 5.2: Mortar Flow Test Results Based on Mineralogy

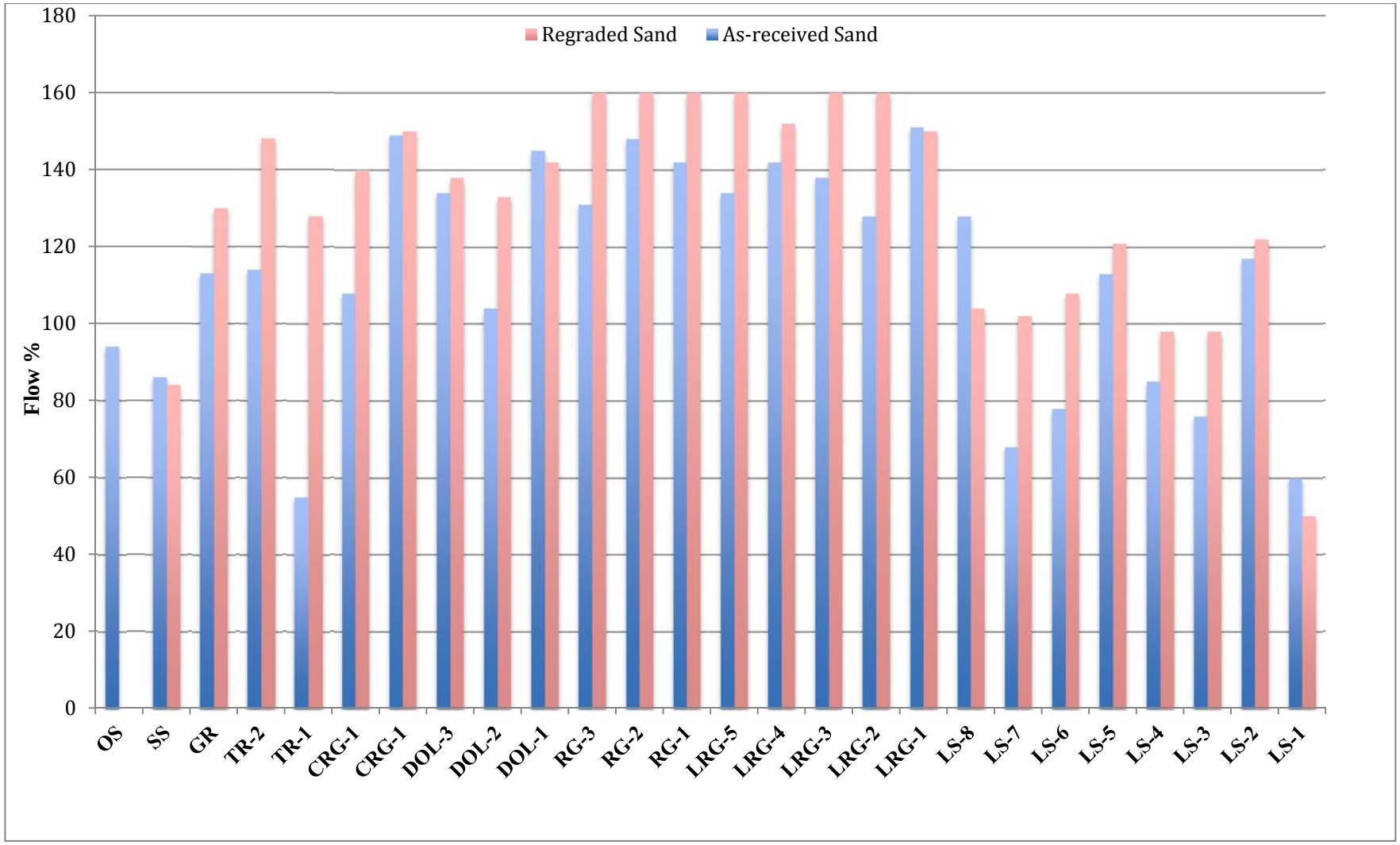

Figure 5.3: Mortar Flow Test Results for All Fine Aggregates

5.4 Mortar Compressive Strength Results

The test of compressive strength of mortars (ASTM C109/C109M) discussed in section 4.10 was performed on the 26 aggregates to evaluate the shape, texture, and angularity by comparing the compressive strength. The test method was conducted both on the as-received sands and on the graded standard sands. Tables 5.2 and 5.3 show the mixture proportions of mortars and the grading requirements for fine aggregate, respectively.

The results of the 7-day-compressive strength of hydraulic cement mortars performed both on the as-received sands and on the regraded sands are shown in Figure 5.5. The regraded sands generally had higher compressive strength. The difference in the 7-day compressive strength between the as-received and the regraded sands varied between 2 and 13%, as shown in Table 5.5. However, the average compressive strength of mortars based on the mineralogy provided no information about the shape and angularity of the fine aggregates, as shown in Figure 5.4.

Table 5.5: Seven-Day Compressive Strength of Mortars Based on Mineralogy

Fine Aggregate Type	As-received sand (psi)	Regraded sand (psi)	% Difference
Limestone	5822	6103	5%
Limestone River Gravel	5636	6031	7%
River Gravel	5538	6214	12%
Dolomite	6249	6998	11%
Crushed River Gravel	5662	5649	0%
Trap Rock	7021	6864	2%
Granite	6668	5869	13%
Sandstone	8035	7858	2%

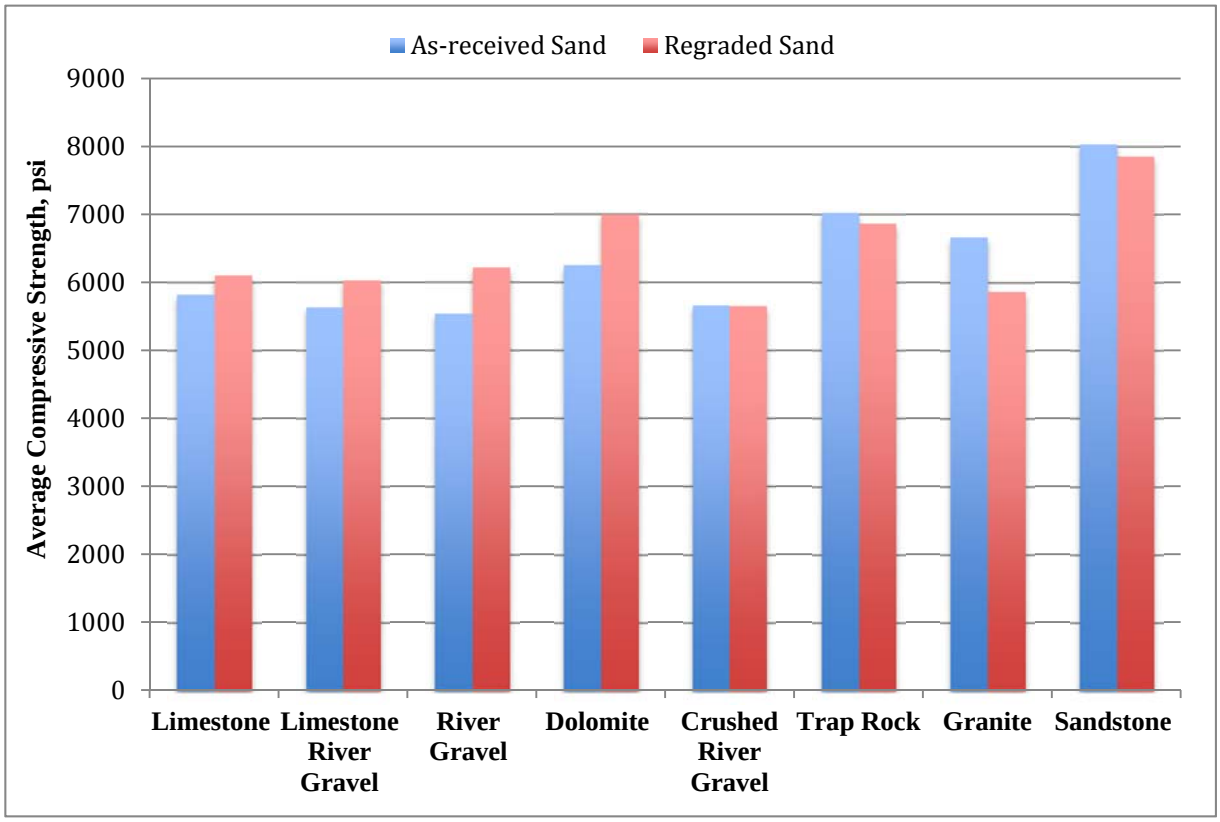

Figure 5.4: Seven-Day Compressive Strength of Mortars Based on Mineralogy

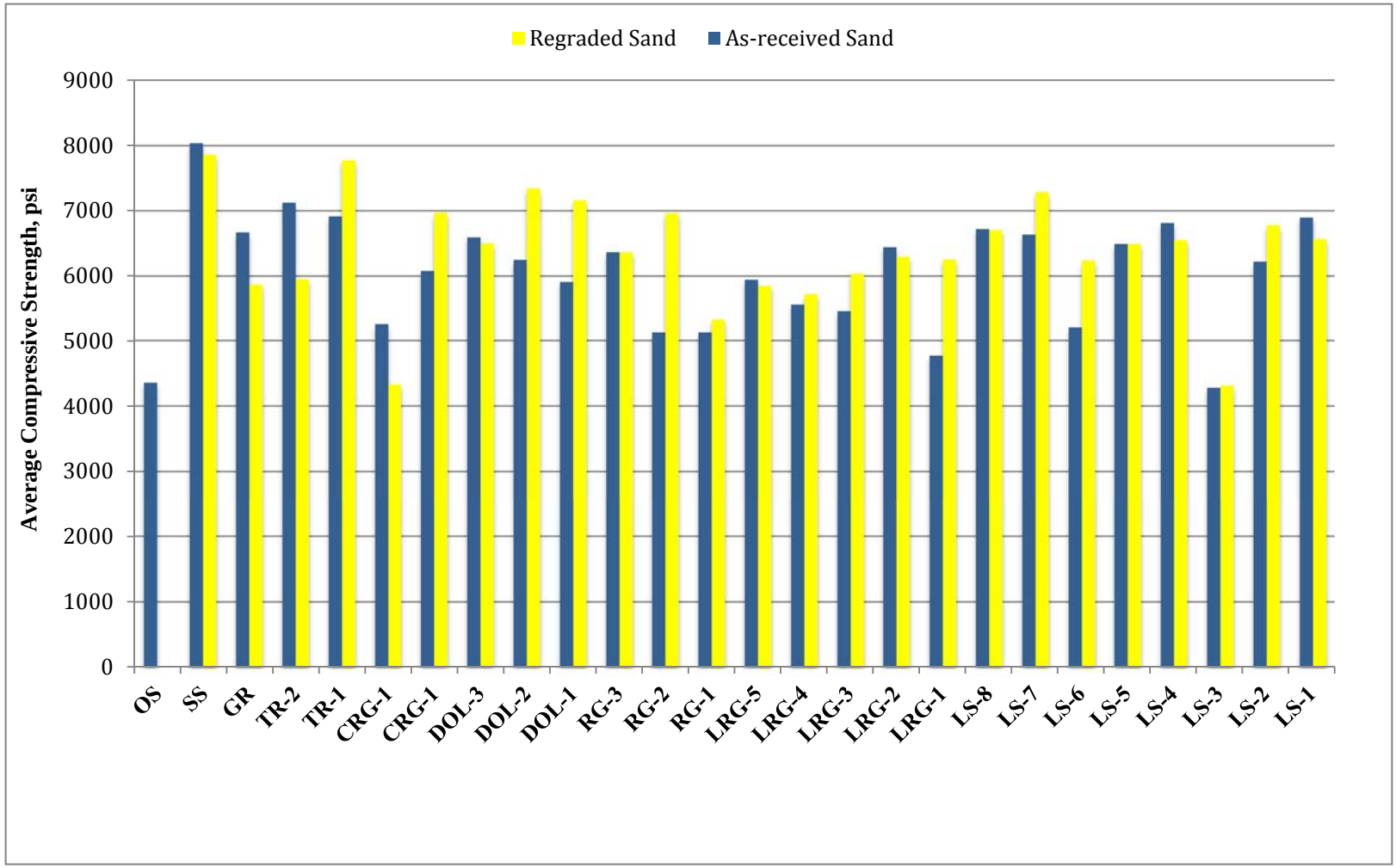

Figure 5.5: Seven-Day Compressive Strength of Mortars for All Fine Aggregates

5.5 AIMS Results

The characteristics of the 26 fine aggregates were evaluated using the AIMS, in accordance with AASHTO TP 81 discussed in section 4.7. The tested size fractions were obtained by sieving the fine aggregates. The form 2-D and angularity of the fine aggregate particles retained on No. 8, No. 16, No. 30, No. 50, No. 100, and No. 200 were evaluated before Micro-Deval (BMD).

The average form 2-D and gradient angularity for all size fractions combined was used as the basis for comparison. Table 5.6 shows the results of form 2-D and angularity based on mineralogy. The river gravel and limestone river gravel had the lowest form 2-D, and the same trend was also observed for the angularity. Thus, it can be concluded that rounded and spherical aggregate particle tend to have lower form 2-D and angularity. It should be emphasized the AIMS was not able to capture the trap rock aggregate particles since they were black.

Table 5.6: AIMS Form 2-D and Angularity Results Based on Mineralogy

Fine Aggregate Type	Form 2-D	Angularity
Limestone	7.10	2695.73
Limestone River Gravel	6.44	2351.92
River Gravel	6.61	2479.53
Dolomite	7.45	2889.77
Crushed River Gravel	6.76	2634.39
Granite	7.15	3304.64
Sandstone	7.15	3243.32

5.6 Camsizer Results

The characteristics of the 26 fine aggregates were evaluated using the Camsizer discussed in section 4.8. A sample of 500 g of each as-received fine aggregate was analyzed to evaluate the sphericity and symmetry of the fine aggregates.

The average sphericity and symmetry for all size fractions combined was used as the basis for comparison. Table 5.7 shows the results of the average sphericity and symmetry based on mineralogy. The limestone river gravel, the river gravel, and the crushed river gravel had the highest level of sphericity, and the same trend was also observed for the symmetry. Thus, it can be concluded that rounded and spherical aggregate particles tend to have higher sphericity and symmetry.

Table 5.7: Camsizer Sphericity and Symmetry Results Based on Mineralogy

Fine Aggregate Type	Sphericity	Symmetry
Limestone	0.81	0.86
Limestone River Gravel	0.85	0.88
River Gravel	0.84	0.88
Dolomite	0.80	0.86
Crushed River Gravel	0.85	0.88
Trap Rock	0.81	0.86
Granite	0.79	0.86
Sandstone	0.79	0.85

5.7 Micro-Deval Test Results

The Micro-Deval test (ASTM D 7428) discussed in section 4.9 was performed on the 26 fine aggregate specimens to determine the resistance of the fine aggregates to abrasion in the presence of water and an abrasive charge.

The results of Micro-Deval loss for the fine aggregates are shown in Figure 5.6; as can be seen, the limestone fine aggregates had the highest Micro-Deval loss. The variations in Micro-Deval loss between the fine aggregates ranged from 5 to 47%.

Table 5.8 shows the results of the average Micro-Deval loss based on mineralogy. The limestone fine aggregate had the highest Micro-Deval loss of 30.45%, while the river gravel fine aggregate had the lowest Micro-Deval loss of 7.73%.

Table 5.8: Micro-Deval Results Based on Mineralogy

Fine Aggregate Type	Micro-Deval
Limestone	30.45
Limestone River Gravel	7.94
River Gravel	7.73
Dolomite	10.30
Crushed River Gravel	7.90
Granite	8.60
Sandstone	21.10

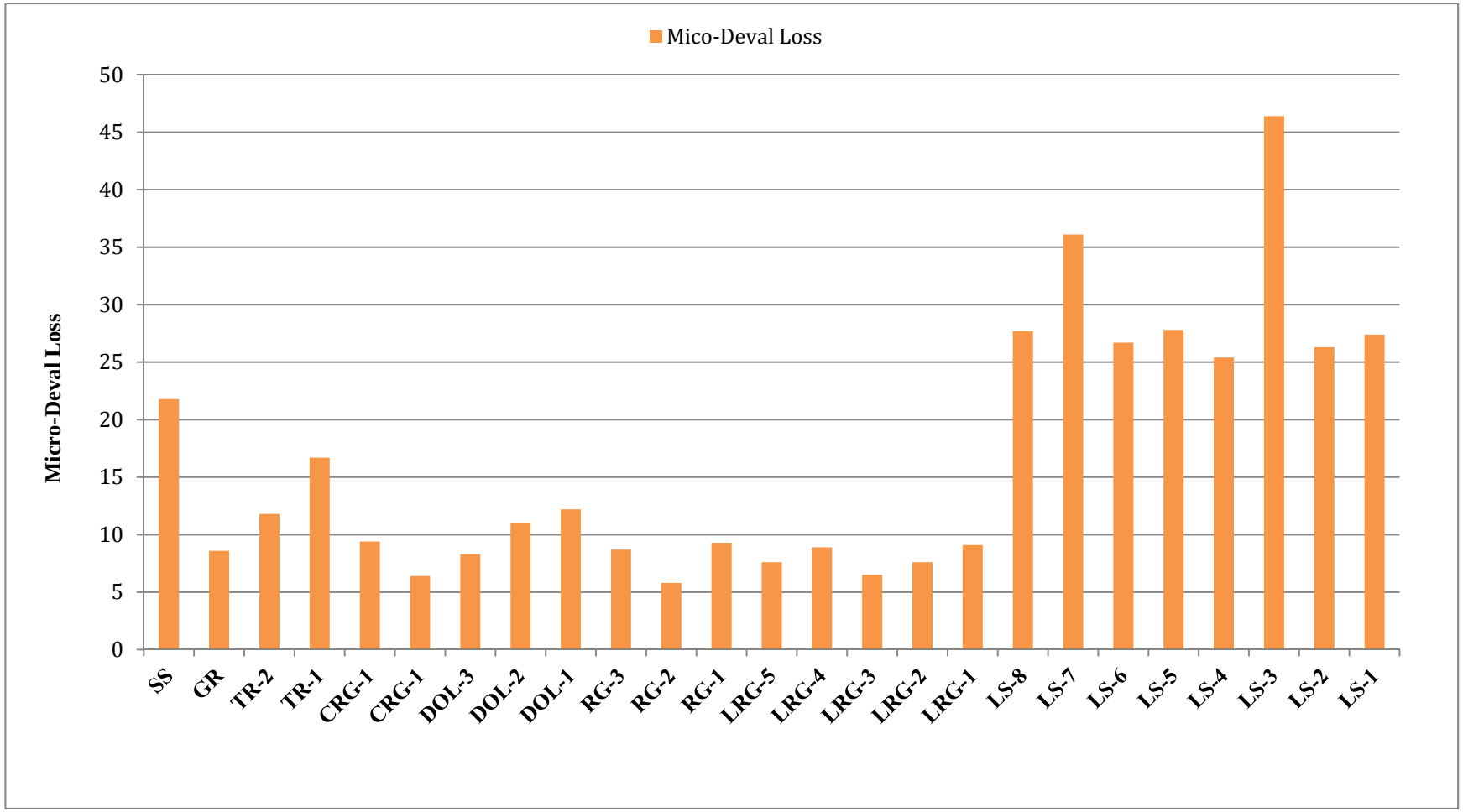

Figure 5.6: Micro-Deval Loss Results Based on Mineralogy

5.8 Flakiness Test Results

The flakiness test (MERO-034) discussed in section 4.6 was used to determine the amount of flaky particles in fine aggregate. The amount of flaky particles was used to assess the angularity of fine aggregates. The flakiness test results of the two size fractions No. 8 and No. 16 were determined.

The results of the flakiness test based on mineralogy are shown in Table 5.9. The limestone and dolomite fine aggregates had the highest level of flaky particles, whereas the river gravel fine aggregates had the lowest level of flaky particles. It can be inferred that rounded and spherical fine aggregate particles tend to have lower levels of flakiness particles, while higher levels of flakiness indicates higher angularity, less sphericity, and rougher surface texture.

Table 5.9: Flakiness Results Based on Mineralogy

Fine Aggregate Type	No. 8	No. 16
Limestone	25.88%	27.11%
Limestone River Gravel	19.20%	25.57%
River Gravel	7.67%	14.37%
Dolomite	28.01%	29.33%
Crushed River Gravel	8.50%	16.83%
Granite	29.20%	65.20%
Sandstone	14.40%	24.10%

5.9 Gradation Analysis Results

The gradation analysis of the 26 fine aggregates was evaluated in terms of percent retained using both the sieve analysis test (ASTM C 136) discussed in section 4.5 and the Camsizer discussed in 4.11. To compare the correlation between the two test methods, a 500-g sample of each fine aggregate was prepared. The same 500-g sample was used both for the sieve analysis test and for the Camsizer to reduce or eliminate the variation in results when using different samples for each test method.

The results of the percentage of the mass retained on each sieve (No. 8, No. 16, No. 30, No. 50, No. 100, and No. 200) for both test methods are shown in Figure 5.7. The results of both tests were approximately the same, with a correlation value R^2 of 0.92.

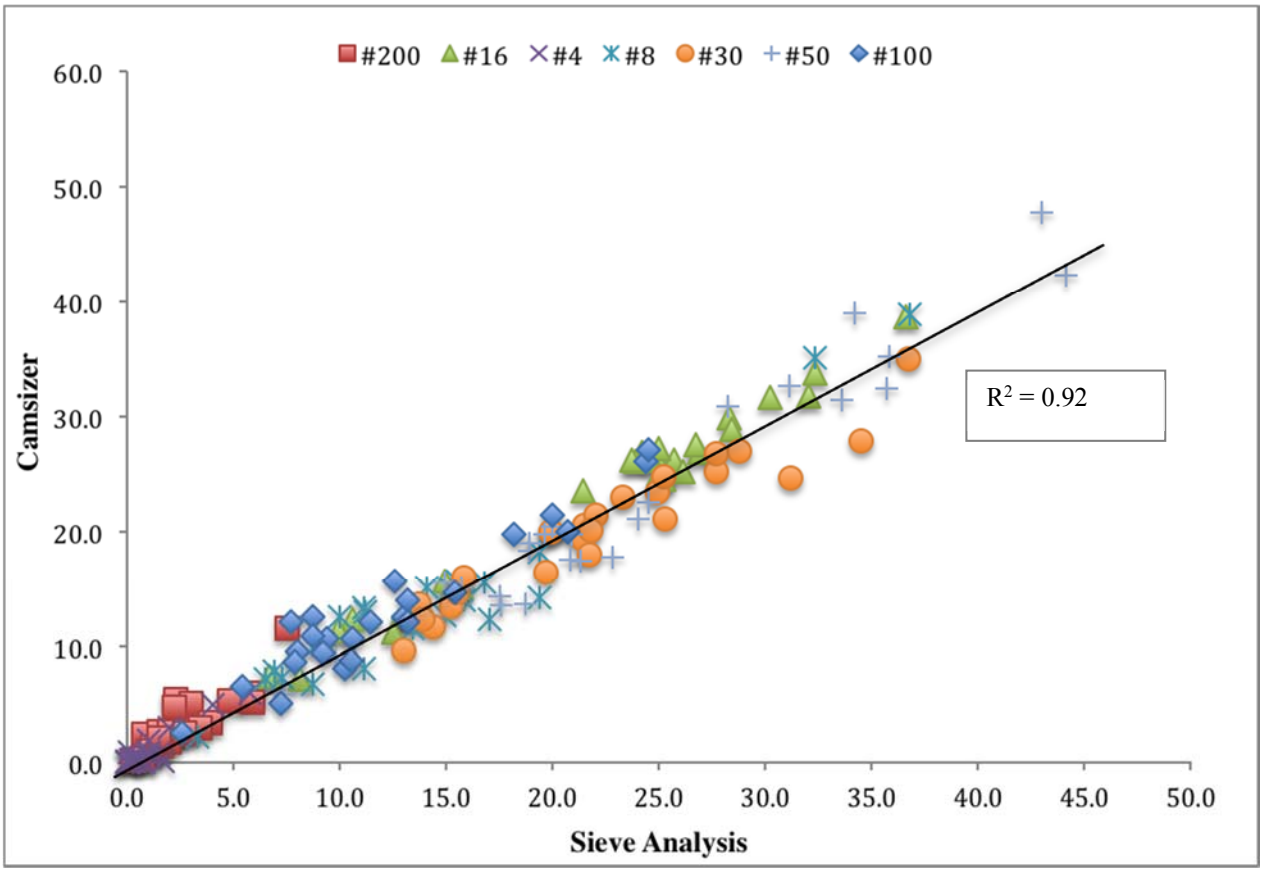

Figure 5.7: Comparison of Gradation Analysis Results from Camsizer and Sieve Analysis Test

The R^2 values for the percentage of the mass retained on each sieve (No. 8, No. 16, No. 30, No. 50, No. 100, and No. 200) using both test methods were 0.94, 0.93, 0.98, 0.92, 0.95, 0.92, and 0.75, respectively. The No. 200 sieve had the lowest R^2 value. There are two reasons for this; first the percentage of the mass retained on No. 200 was in the range of 0.2 to 5%, which means a small change in the mass retained on No. 200 would have a significant impact on the percentage of the mass retained on No. 200 unlike with the other sieves; second there is a possibility of losing finer materials when sieving. It is believed that the results of gradation analysis obtained by Camsizer are more accurate than that of the sieve analysis test since the variations in the results when the tested was repeated on the same sample was less for the Camsizer compared to the sieving test, and the amount of finer materials lost when sieving was performed was higher than the Camsizer.

5.9.1 The Effect of Size on Gradation Analysis

To investigate the effect of size on the result of gradation analysis, two different samples of each fine aggregate were tested using the Camsizer. The first sample was 20 to 30 g and the second sample was 500 g. The results showed that the size of the sample tested had a significant impact on the results of gradation analysis. The sieve analysis test results were used as the basis for comparison between the two sizes. The R^2 values between the Camsizer and sieve analysis test were 0.48 for the smaller sample and 0.93 for the 500-g sample. It should be emphasized that the average time required to run the test was 2 to 3 min for the smaller sample and 28 to 35 min for the 500-g sample.

5.10 General Correlations

Laboratory test results were compared to find out whether trends exist between the different tests.

5.10.1 AIMS versus Flakiness Test

The results of the flakiness test versus AIMS form 2-D for the fine aggregates retained on No. 8 and No. 16 obtained by sieving are shown in Figure 5.8 and Figure 5.9, respectively. As can be seen, little correlation existed between AIMS form 2-D and the flakiness test, especially with No.8. The R^2 values for the fine aggregates retained on No. 8 and No. 16 were found to be 0.20 and 0.28, respectively.

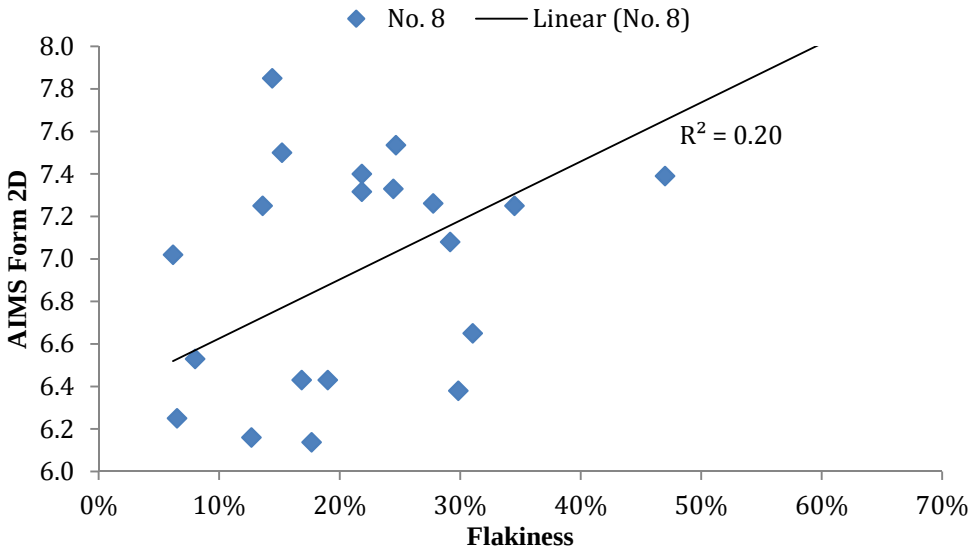

Figure 5.8: AIMS Form 2-D versus Flakiness (No. 8)

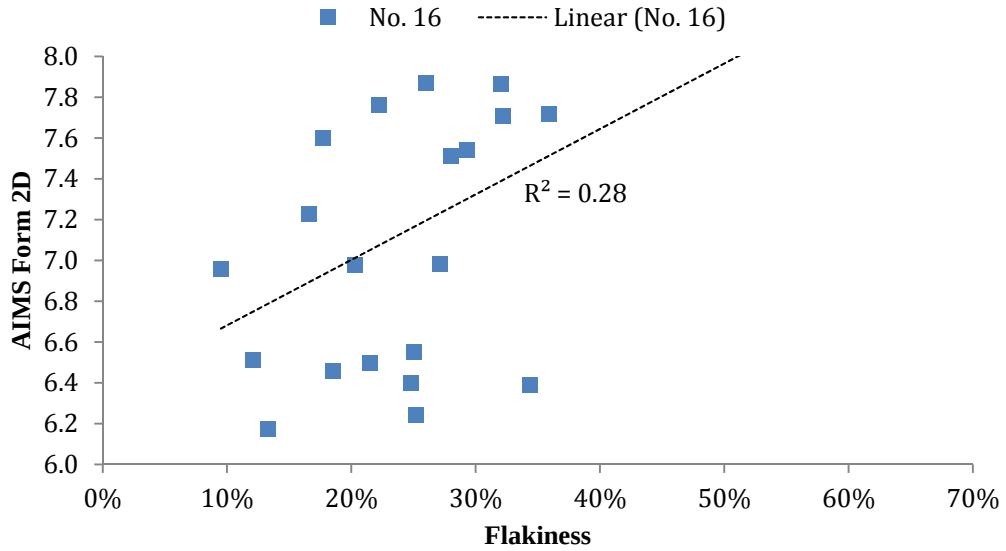

Figure 5.9: AIMS Form 2-D versus Flakiness (No. 16)

The results of the flakiness test versus the angularity for the two size fractions No. 8 and No. 16 are shown in Figure 5.10 and Figure 5.11. As can be seen, almost no correlation existed between AIMS angularity and the flakiness for the fine aggregates retained on No. 8. . The R^2 values for the fine aggregates retained on No. 8 and No. 16 were 0.08 and 0.16, respectively. The flakiness results of the fine aggregates for sieve No. 16, thus, gave a slightly higher R^2 value than that of No. 8.

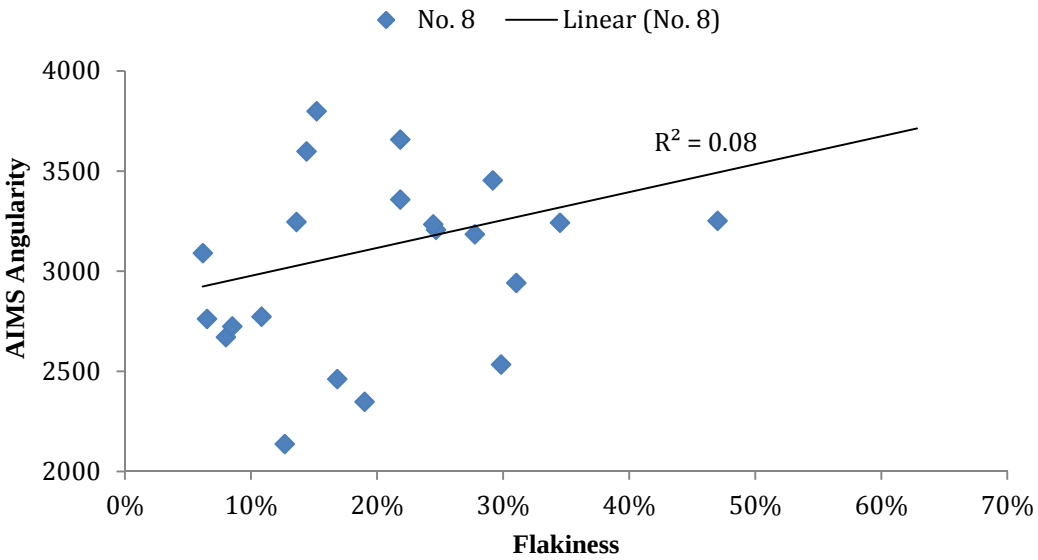

Figure 5.10: AIMS Angularity versus Flakiness (No. 8)

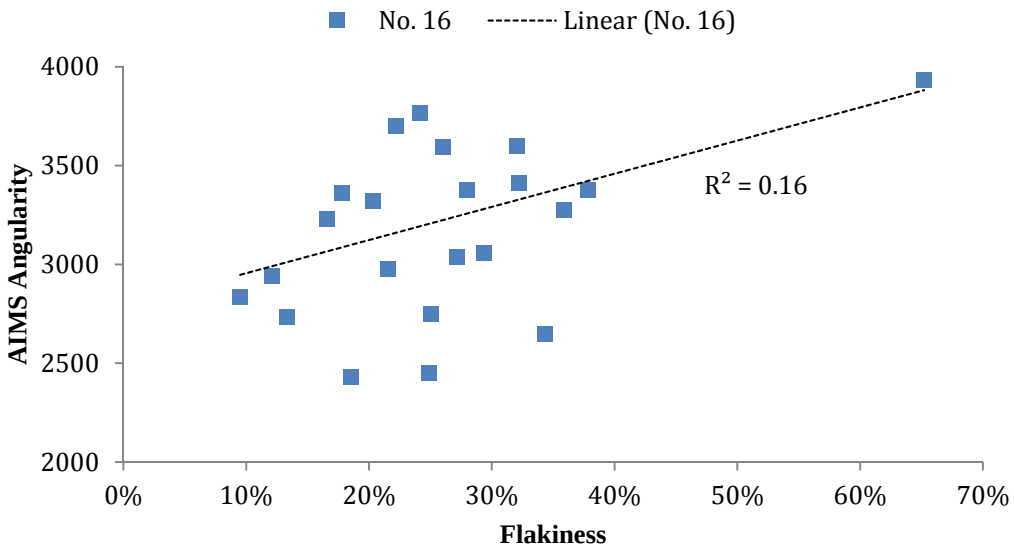

Figure 5.11: AIMS Angularity versus Flakiness (No. 16)

5.10.2 Camsizer versus Flakiness Test

The results of the flakiness test versus Camsizer sphericity for the two size fractions No. 8 and No. 16 are shown in Figure 5.12 and Figure 5.13, respectively. The two size fractions were obtained by sieving. The R^2 values for the fine aggregates retained on No. 8 and No. 16 were 0.34 and 0.43, respectively. As can be seen, very little correlation existed between the results of Camsizer sphericity and the flakiness test for the No. 8 sieve, whereas the correlation increased to 0.43 for the No. 16 sieve.

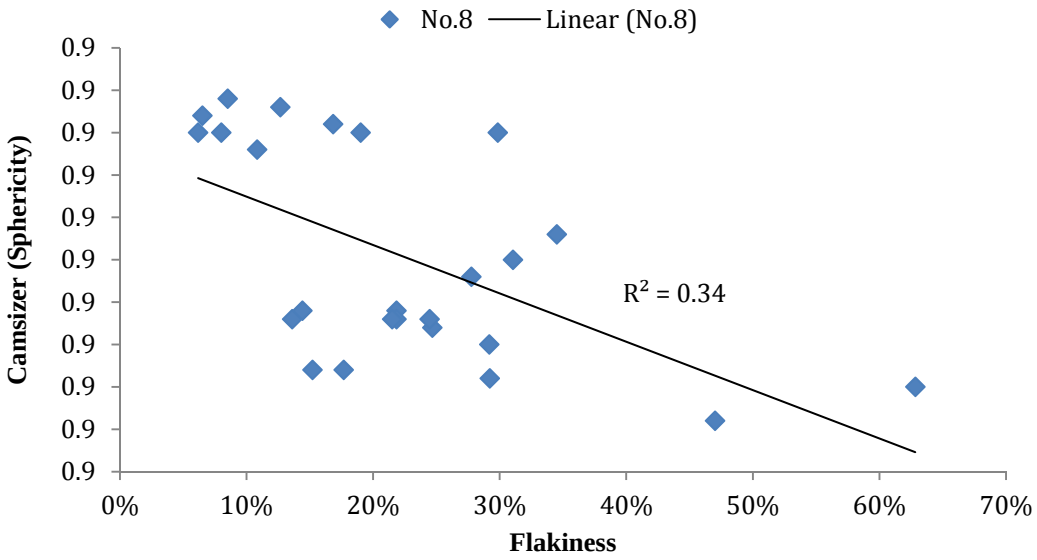

Figure 5.12: Camsizer Sphericity versus Flakiness (No. 8)

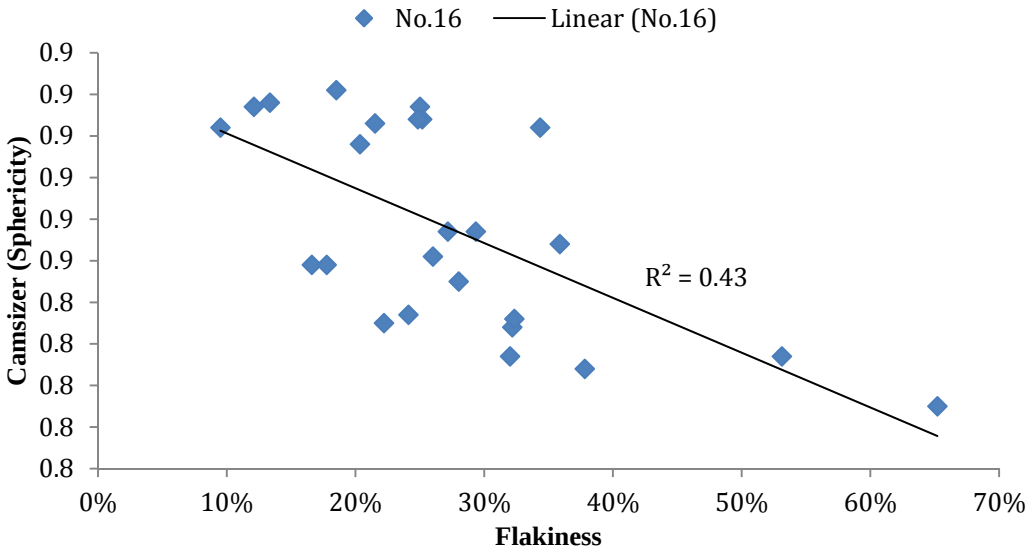

Figure 5.13: Camsizer Sphericity versus Flakiness (No. 16)

The results of the flakiness test versus Camsizer symmetry for the two size fractions No.8 and No.16 are shown in Figure 5.14 and Figure 5.15, respectively. The R^2 values for the fine aggregates retained on No. 8 and No. 16 were the same, 0.35.

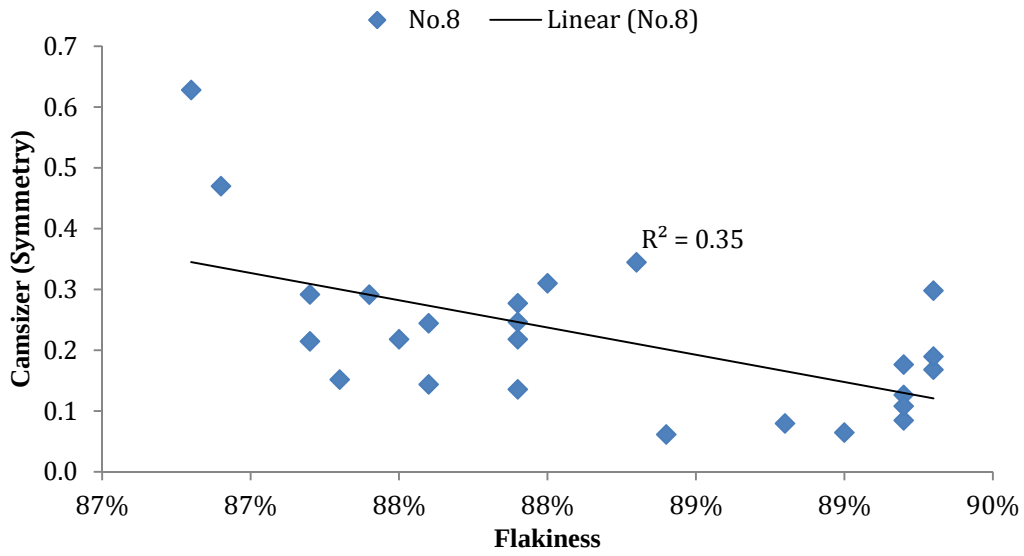

Figure 5.14: Camsizer Symmetry versus Flakiness (No. 8)

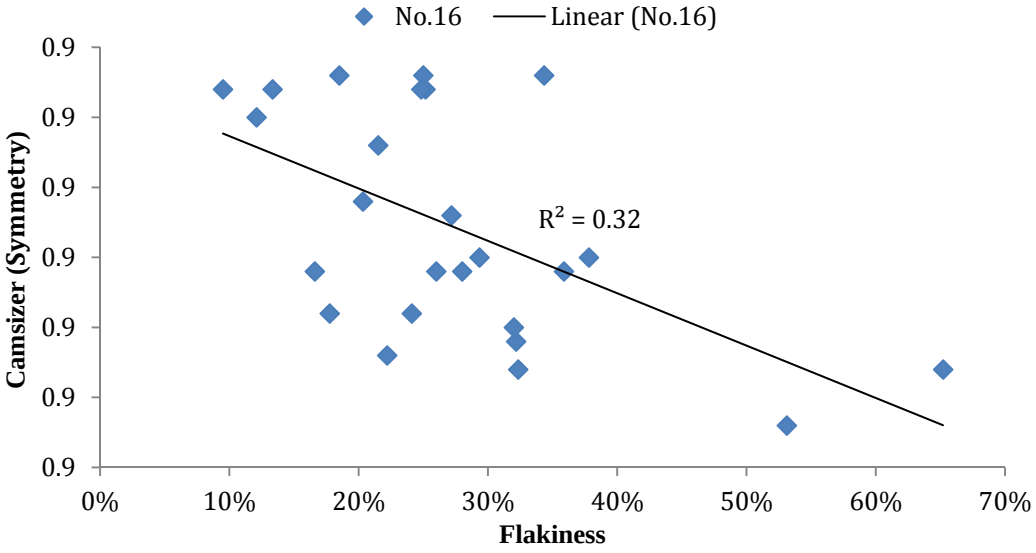

Figure 5.15: Camsizer Symmetry versus Flakiness (No. 16)

5.10.3 AIMS versus Uncompacted Void Test

The average form 2-D and angularity for all size fractions combined was used as the basis for comparison between the two tests. Table 5.10 shows the correlation between AIMS and uncompacted void test. Methods A and B correlated well with the AIMS form 2-D, whereas Method C had little correlation; the same trend was also observed with angularity, though with a lower R^2value.

Table 5.10: Correlation between AIMS and Uncompacted Void Test

	R^2- Method A	R^2- Method B	R^2- Method C
Form 2-D	0.66	0.66	0.29
Angularity	0.46	0.44	0.14

5.10.4 Camsizer versus Uncompacted Void Test

The average sphericity and symmetry for all size fractions combined was used as the basis for comparison between the two tests. Table 5.11 shows the correlation between the Camsizer and the uncompacted void test. Methods A and B correlated well with both sphericity and symmetry, whereas Method C had little correlation.

Table 5.11: Correlation between AIMS and Uncompacted Void Test

	R^2- Method A	R^2- Method B	R^2- Method C
Sphericity	0.64	0.67	0.26
Symmetry	0.60	0.66	0.20

5.10.5 AIMS versus Mortar Flow Test

The average form 2-D and angularity for all size fractions combined was used as the basis for comparison between the two tests. Table 5.12 shows the correlation between the AIMS and the mortar flow test. Almost no correlation was observed between the AIMS and the mortar flow test. The correlation tends to increase slightly with regraded sands.

Table 5.12: Correlation between AIMS and Mortar Flow Test

	R^2- As-received sand	R^2- Regraded sand
Form 2-D	0.10	0.19
Angularity	0.05	0.12

5.10.6 Camsizer versus Mortar Flow Test

The average sphericity and symmetry for all size fractions combined was used as the basis for comparison between the two tests. Table 5.13 shows the correlation between Camsizer and mortar flow test. Little correlation was observed between AIMS and mortar flow test. The correlation tends to increase with regraded sands.

Table 5.13: Correlation between AIMS and Mortar Flow Test

	R^2- As-received sand	R^2- Regraded sand
Sphericity	0.20	0.25
Symmetry	0.27	0.33

5.10.7 AIMS versus Compressive Strength of Mortars

The average form 2-D and angularity for all size fractions combined was used as the basis for comparison between the two tests. Table 5.12 shows the correlation between the AIMS and the compressive strength of mortars. Little correlation was observed between the AIMS and the compressive strength of mortars. The correlation tends to decrease slightly with regraded sands.

Table 5.14: Correlation between AIMS and Mortar Compressive Strength Test

	As-received sand	Regraded sand
Form 2-D	0.16	0.12
Angularity	0.25	0.08

5.10.8 Camsizer versus Compressive Strength of Mortars

The average sphericity and symmetry for all size fractions combined was used as the basis for comparison between the two tests. Table 5.13 shows the correlation between Camsizer and compressive strength of mortars. Almost no correlation was observed between AIMS and compressive strength of mortars. The correlation tends to decrease with regraded sands.

Table 5.15: Correlation between AIMS and Mortar Compressive Strength Test

	As-received sand	Regraded sand
Sphericity	0.16	0.05
Symmetry	0.17	0.08

5.10.9 AIMS versus Camsizer

The results of the AIMS form 2-D versus Camsizer sphericity for the two size fractions No. 8 and No. 16 obtained by sieving are shown in Figure 5.16 and Figure 5.17, respectively. As can be seen, excellent correlations existed between the results of the Camsizer sphericity and the AIMS form 2-D for the two size fractions No. 8 and No. 16, with R^2 values of 0.89 and 0.87, respectively.

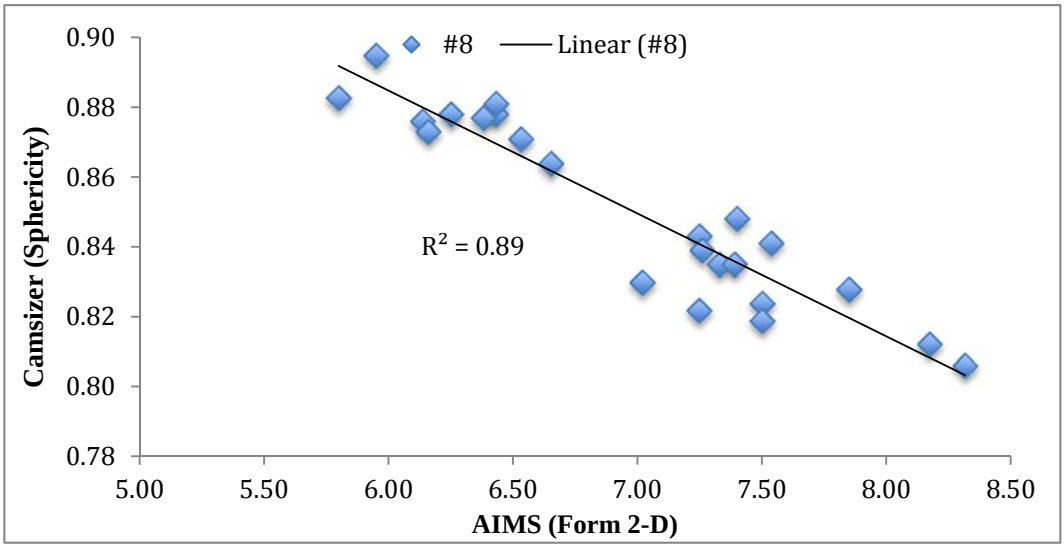

Figure 5.16: Camsizer Sphericity versus AIMS Form 2-D (No. 8)

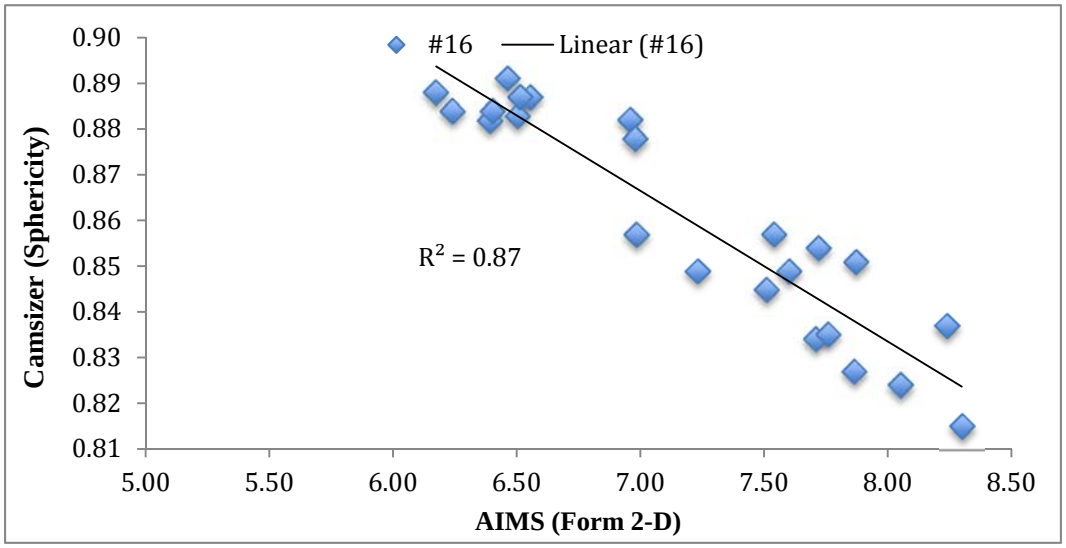

Figure 5.17: Camsizer Sphericity versus AIMS Form 2-D (No. 16)

The results of the AIMS angularity versus Camsizer symmetry are shown in Figure 5.17 and Figure 5.18, respectively. As can be seen, excellent correlations exist between the results of the Camsizer symmetry and the AIMS angularity for the two size fractions No. 8 and No. 16, with R^2 values of 0.83 and 0.82, respectively.

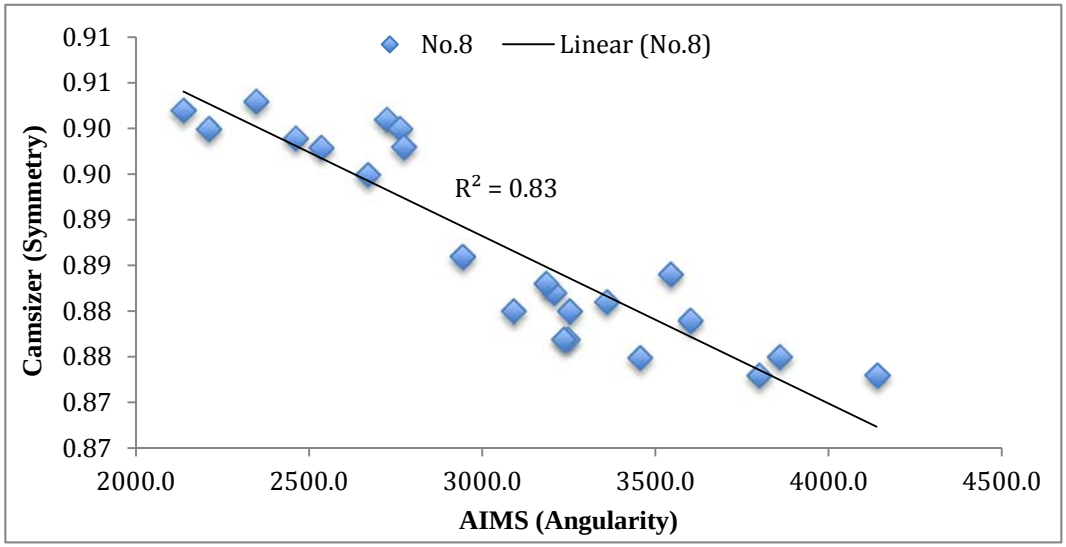

Figure 5.18: Camsizer Symmetry versus AIMS Form 2-D (No. 8)

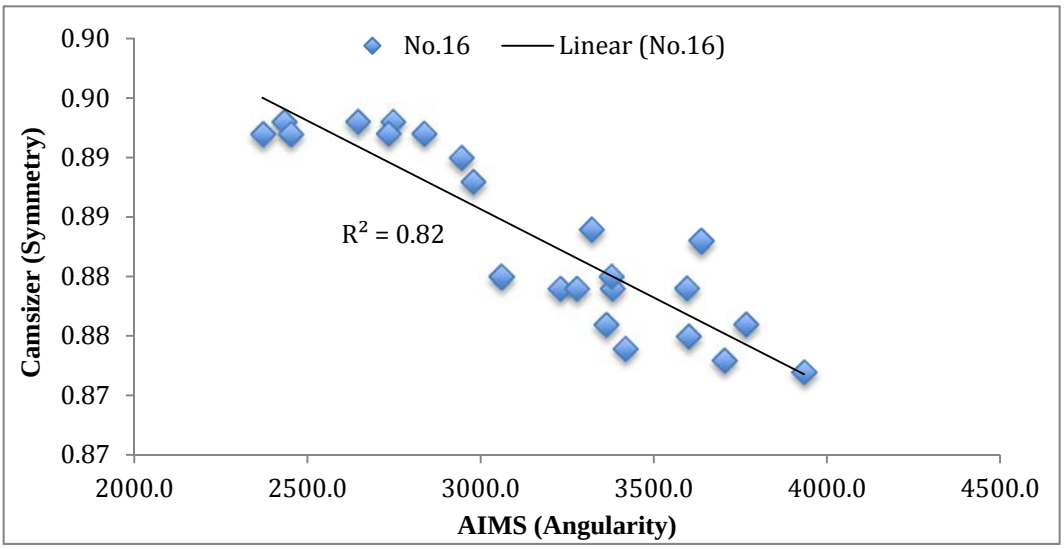

Figure 5.19: Camsizer Symmetry versus AIMS Angularity (No. 16)

5.10.10 Micro-Deval Test versus Mortar Flow Test

Figure 5.20 shows the relationship between the Micro-Deval test and the mortar flow test. As can be seen, the R^2 values between the Micro-Deval loss and the flow for the as-received sands and for the regraded sands were 0.59 and 0.77, respectively. It can be concluded that regraded sands having a flow percentage higher than or equal to 130 tend to have Micro-Deval loss of less than or equal to 12%. On the other hand, values of Micro-Deval loss greater than 20% were observed when the flow was below 110%, as shown in Figure 5.21.

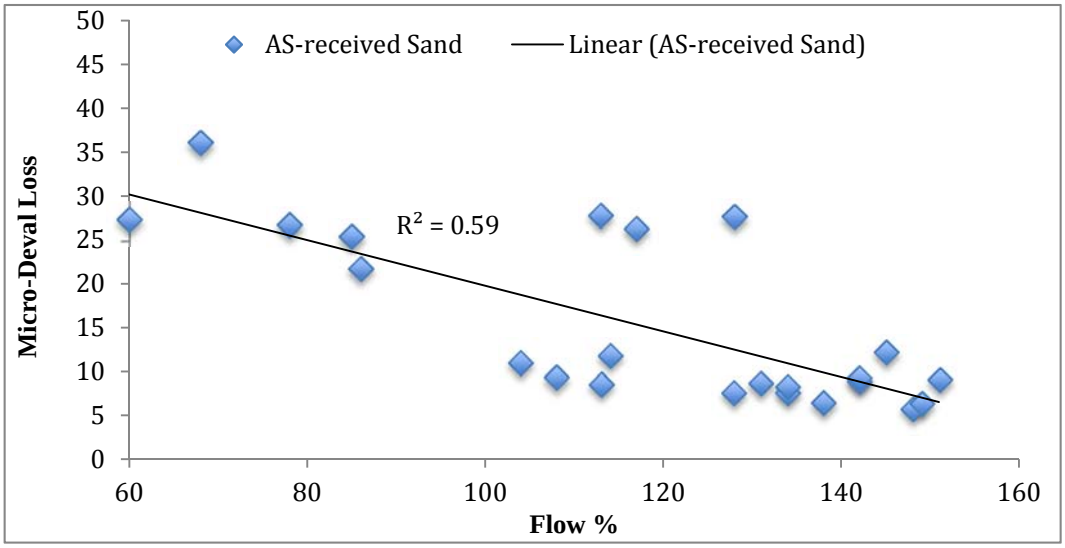

Figure 5.20 Micro-Deval Test versus Mortar Flow Test for the As-received Sands

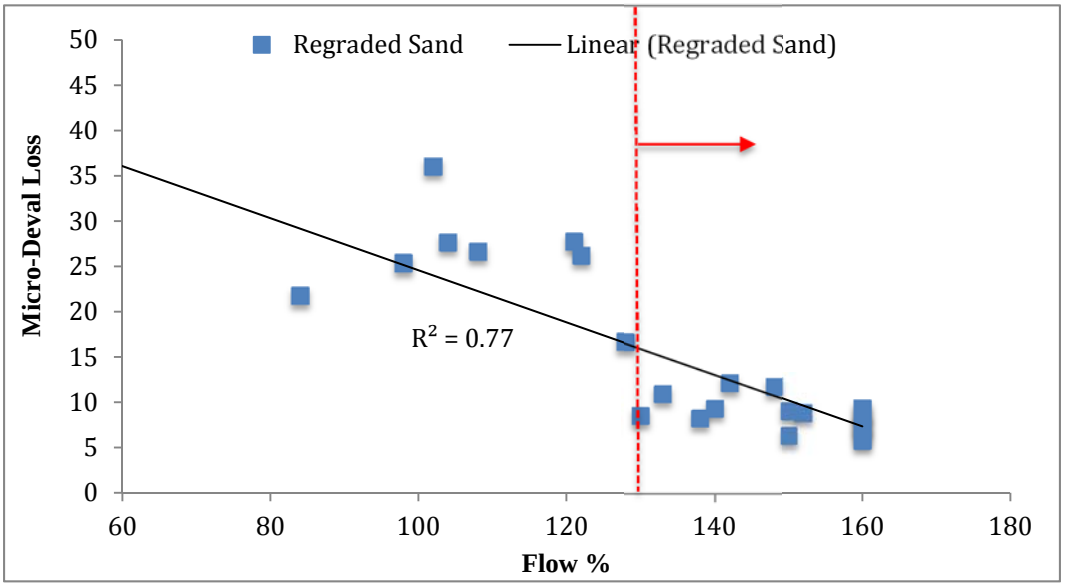

Figure 5.21 Micro-Deval Test versus Mortar Flow Test for The Regraded Sands

5.10.11 Micro-Deval Test versus AIMS

The Micro-Deval test had no correlation with the AIMS. The change in the results of BMD and AMD for both form 2-D and angularity was not consistent. This means some fine aggregates had a higher value of BMD both for form 2-D and for angularity than AMD, while other fine aggregates had a lower value.

5.10.12 Sand Equivalent Test versus Blue Methylene Test

The relative amount of harmful fine dust or clay-like particles in fine aggregates was evaluated using ASTM D 2419 (Standard Test Method for Sand Equivalent Value of Soils and Fine Aggregate) and he ASTM C 837 (Standard Test Method for Methylene Blue Index of Clay). Figure 5.22 shows a good correlation between the two test methods, with an R^2 value of 0.53.

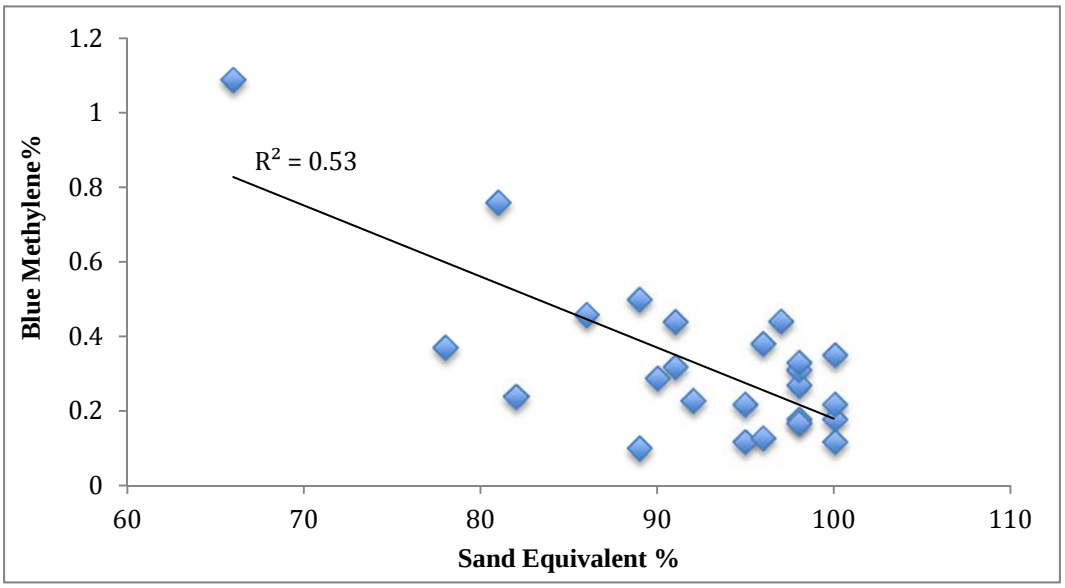

Figure 5.22 Sand Equivalent Test versus Blue Methylene Test

5.11 Comparison between Approved and Non-approved Fine Aggregates

This section evaluates and compares the results of non-approved fine aggregates with the approved fine aggregates to see whether some non-approved fine aggregates can be successfully used. The following fine aggregates are classified as non-approved fine aggregates in accordance with TxDOT's specifications (ITEM 421): LS-3, LS-5, LS-8, TR-1, TR-2, and SS.

The TxDOT's specifications (ITEM 421) require that fine aggregates satisfy certain criteria when the following tests are conducted: a visual inspection test, the deleterious materials test (Tex-413-A), the organic impurities test (Tex-408-A), the acid insoluble test (Tex-612-J), the sieve analysis test (Tex-401-A), the sand equivalent test (Tex-203-F), and the fineness modulus test (Tex-402-A).

The non-approved fine aggregates had Micro-Deval loss values higher than 21%, except for TR-1 and TR-2. However, some of the approved fine aggregates had high Micro-Deval loss values. For instance, LS-1 and LS-5 had Micro-Deval loss values of 27% and 36%, respectively.

The results of the AIMS form 2-D and angularity differed little between the approved and non-approved fine aggregates. The AIMS was not able to evaluate TR-1 and TR-2 because they were black.

The Camsizer sphericity and symmetry results also differed little between the approved and non-approved fine aggregates.

Among all the non-approved fine aggregates, LS-5, LS-8, and SS had values of uncompacted void similar to those of the approved fine aggregates. TR-1 and TR-2,

however, had the highest uncompacted void content of all the approved and non-approved fine aggregates.

The non-approved fine aggregates generally had lower flow compared to the approved ones. The mortar flow was 84% for the as-received SS and 86% for the regraded SS. However, the compressive strength results were variable. This means that some of the non-approved fine aggregates had higher values on the compressive strength test, while other fine aggregates had a lower value compared to the approved fine aggregates.

LS-3 had the highest absorption at 7.2%, while the other non-approved fine aggregates had absorption values similar to those of the approved fine aggregates. TR-1 and TR had the highest specific gravity, 3.08.

TR-1 and LS-3 had the highest blue methylene content at 1.09% and 0.67% respectively, while the other non-approved fine aggregates had blue methylene values similar to those of the approved fine aggregates.

The non-approved fine aggregates had sand equivalent values similar to those of the approved fine aggregates.

Chapter 6: Summary and Conclusions

6.1 Summary

The objectives of this study were achieved by evaluating the characteristics of 26 fine aggregates (shape, angularity, and surface texture) using both direct and indirect test methods. Laboratory test results were compared to discover the trends between the different tests. The correlation value (R^2) between the different test methods helped identify which test methods could be recommended for use. The non-approved fine aggregates on TxDOT's list were analyzed and compared to those of the approved fine aggregates to see whether they could be successfully used.

6.1 Conclusion

The testing performed in this study evaluated the characteristics of fine aggregates (shape, angularity, and surface texture). Based on the results of this study, the following conclusions can be drawn:

1- The mortar flow test method was able to evaluate the characteristics of fine aggregates (shape and surface texture). The mortar flow test can be time-intensive if regraded sands are used. Interestingly, the flow of regraded sands can provide valuable information about the resistance of fine aggregate to. The mortar flow test for the regraded sands seems to correlate closely with the Micro-Deval test.

2- The compressive strength of mortars test did not yield any indication of the characteristics of a fine aggregate. However, higher compressive strength was generally observed for the regraded sands compared to the as-received sand.

3- The flakiness test provides little information about the characteristics of fine aggregate compared to other indirect test methods. The flakiness test did not correlate well with the AIMS and the Camsizer. Thus, it is not recommended for use.

4- The uncompacted void content test (Method A and Method B) was found to be the best indirect test for evaluating the characteristics of fine aggregates (shape and texture). Method C; however, failed to provide any indication of shape and texture. Method B's drawback is that it is more time-consuming, since the test is performed on three individual size fractions. In addition, the correlations between the results of Methods A and B with the results of the AIMS and the Camsizer were similar. Therefore, Method A can be used with confidence.

5- The AIMS is capable of measuring the characteristics of fine aggregate by evaluating form 2-D and angularity. However, the AIMS failed to capture the trap rock fine aggregate particles because the particles were black.

6- The Camsizer can evaluate the characteristics of fine aggregates by measuring sphericity and angularity, and it can also perform a gradation analysis of fine aggregate. However, the size of the sample was found to play an important role in obtaining accurate results.

7- The accuracy of the AIMS and the Camsizer was evaluated by comparing the results of each test. It was observed that excellent correlations exist between the

two systems, even though the mathematical formulas for evaluating the fine aggregate characteristics are not the same.

8- The Micro-Deval loss was significant for the limestone fine aggregates compared to that of other fine aggregates.

9- The blue methylene test correlated with the sand equivalent test. This would encourage the use of the blue methylene test, since it is practical and simple.

10- The non-approved fine aggregates were compared with the approved fine aggregates. It was found that both LS-5 and LS-8 had good results—even better than the results of some of the approved fine aggregates. Thus, they could be successfully used.

6.3 Directions for Future Research

As stated previously, the mortar flow test (ASTM C 1437) indirectly evaluates the shape and texture of fine aggregates by comparing workability. The mortar flow test is based on fixed water-cement and fine aggregate-cement ratios of 0.485 and 2.75, respectively. The mortar flow test does not account for the absorption of fine aggregates. It would be interesting to see how much improvement in quantifying shape and texture of fine aggregates can be achieved when using different water-cement and fine aggregate-cement ratios and accounting for the absorption of fine aggregates.

The AIMS and the Camsizer are direct tests used to evaluate the characteristics of fine aggregate. More research is required to determine whether the AIMS and the Camsizer can measure the shape, angularity, and surface texture of fine aggregates

crushed at different speeds and with different crushers. This would encourage the use of the AIMS and the Camsizer in practice as a form of quality control.

Appendix A: Fine Aggregate Samples

Figure A.1: Standard Graded Fine Aggregate Sample, Left-to- right, SS and RG-3

Figure A.2: Standard Graded Fine Aggregate Sample, Left-to- right, DOL-3 and LGR-5

Figure A.3: Standard Graded Fine Aggregate Sample, Left-to- right, TR-1 and GR

Figure A.4: Standard Graded Fine Aggregate Sample, Left-to- right, LS-1 and LS-4

Figure A.5: Standard Graded Fine Aggregate Sample, Left-to- right, LS-8 and LS-7

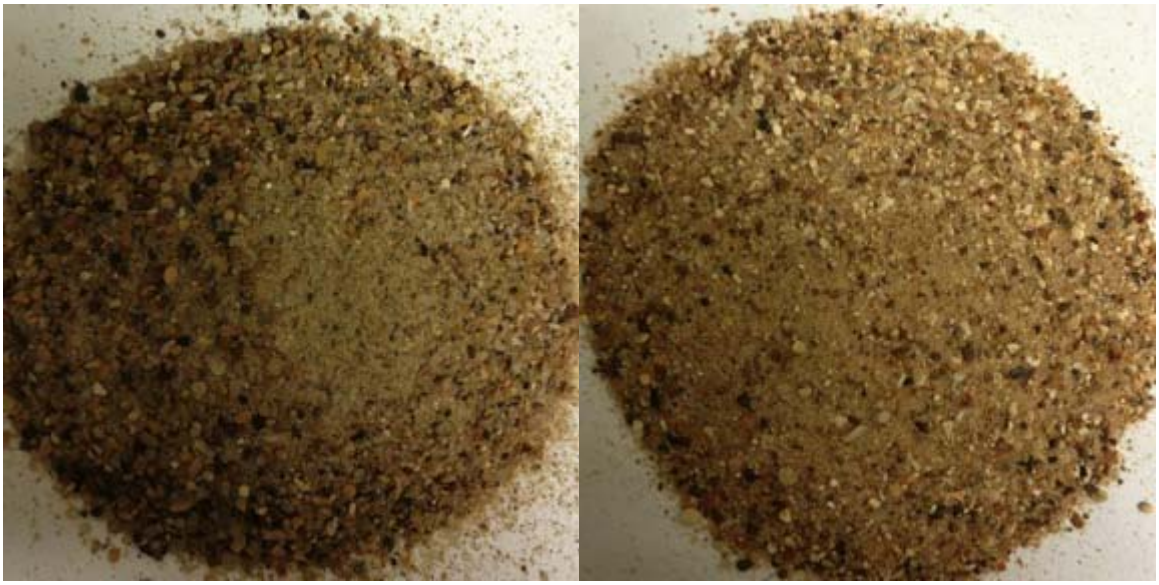

Figure A.6: Standard Graded Fine Aggregate Sample, Left-to- right, LRG-4 and LRG-1

Figure A.7: Standard Graded Fine Aggregate Sample, Left-to- right, RG-1 and DOL-1

Figure A.8: Standard Graded Fine Aggregate Sample, Left-to- right, LS-2 and LS-5

Figure A.9: Standard Graded Fine Aggregate Sample, Left-to- right, CRG-1 and LS-3

Figure A.10: Standard Graded Fine Aggregate Sample, Left-to- right, LRG-2 and TR-2

Figure A.11: Standard Graded Fine Aggregate Sample, Left-to- right, DOL-2 and LRG-3

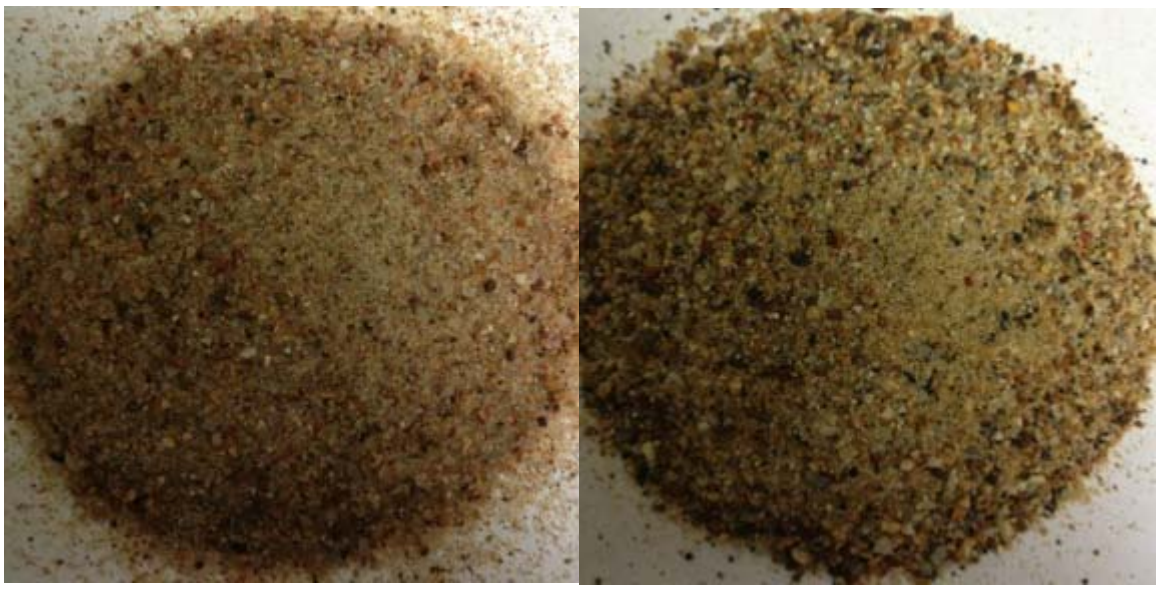

Figure A.12: Standard Graded Fine Aggregate Sample, Left-to- right, CRG-1 and RG-2

Figure A.13: Standard Graded Fine Aggregate Sample, Left-to- right, LS-6 and OS

Appendix B: Presentation of Results for All Testing

Table B.1: Physical Properties of Fine Aggregates

Designation	AIR %	SG	ABS %
LS-1	4	2.56	2.4
LS-2	4	2.54	3.3
LS-3	4	2.41	7.2
LS-4	4	2.58	2.1
LS-5	1	2.63	1
LS-6	4	2.58	2.1
LS-7	5	2.6	2.2
LS-8	8	2.64	1.8
LRG-1	87	2.64	0.7
LRG-2	79	2.62	1
LRG-3	84	2.64	0.7
LRG-4	76	2.62	1.7
LRG-5	80	2.61	2.1
RG-1	88	2.61	0.8
RG-2	100	2.57	1.1
RG-3	88	2.62	0.6
DOL-1	4	2.8	0.5
DOL-2	12	2.74	1.4
DOL-3	21	2.81	0.5
CRG-1	99	2.63	0.4
CRG-1	92	2.63	0.6
TR-1	83	3.08	0.6
TR-2	89	3.08	0.8
GR	96	2.67	0.4
SS	63	2.62	0.8

Table B.2: Sand Equivalent Test Results

Designation	Sand Equivalents %
LS-1	91
LS-2	95
LS-3	81
LS-4	90
LS-5	78
LS-6	95
LS-7	86
LS-8	89
LRG-1	98
LRG-2	96
LRG-3	97
LRG-4	98
LRG-5	98
RG-1	100
RG-2	100
RG-3	100
DOL-1	89
DOL-2	98
DOL-3	96
CRG-1	100
CRG-1	91
TR-1	66
TR-2	98
GR	92
SS	82

Table B.3: Blue Methylene Test Results

Designation	**Blue Methylene %**
LS-1	0.32
LS-2	0.22
LS-3	0.76
LS-4	0.29
LS-5	0.37
LS-6	0.12
LS-7	0.46
LS-8	0.5
LRG-1	0.27
LRG-2	0.38
LRG-3	0.44
LRG-4	0.31
LRG-5	0.33
RG-1	0.35
RG-2	0.12
RG-3	0.18
DOL-1	0.1
DOL-2	0.18
DOL-3	0.13
CRG-1	0.22
CRG-1	0.44
TR-1	1.09
TR-2	0.17
GR	0.23
SS	0.24

Table B.4: Micro-Deval Test Results

Designation	Micro-Deval Loss %
LS-1	27.4
LS-2	26.3
LS-3	46.4
LS-4	25.4
LS-5	27.8
LS-6	26.7
LS-7	36.1
LS-8	27.7
LRG-1	9.1
LRG-2	7.6
LRG-3	6.5
LRG-4	8.9
LRG-5	7.6
RG-1	9.3
RG-2	5.8
RG-3	8.7
DOL-1	12.2
DOL-2	11
DOL-3	8.3
CRG-1	6.4
CRG-1	9.4
TR-1	16.7
TR-2	11.8
GR	8.6
SS	21.8

Table B.5: Flakiness Test Test Results

Designation	No.8	No.16
LS-1	13.6%	16.6%
LS-2	24.7%	26.0%
LS-3	34.5%	27.2%
LS-4	24.5%	17.8%
LS-5	29.2%	32.2%
LS-6	31.0%	29.3%
LS-7	27.8%	35.9%
LS-8	21.8%	32.0%
LRG-1	16.8%	25.0%
LRG-2	17.7%	25.2%
LRG-3	19.0%	18.5%
LRG-4	29.8%	34.3%
LRG-5	12.7%	24.8%
RG-1	8.0%	21.5%
RG-2	8.5%	9.5%
RG-3	6.5%	12.1%
DOL-1	21.8%	28.0%
DOL-2	47.0%	37.8%
DOL-3	15.2%	22.2%
CRG-1	10.8%	13.3%
CRG-1	6.2%	20.3%
TR-1	21.5%	32.3%
TR-2	62.8%	53.1%
GR	29.2%	65.2%
SS	14.4%	24.1%

Table B.6: Camsizer Sphericity Results

Designation	No. 8	No. 16	No. 30	No. 50	No. 100	No. 200	Average
LS-1	0.81	0.85	0.87	0.72	0.76	0.84	0.81
LS-2	0.80	0.84	0.87	0.74	0.78	0.84	0.81
LS-3	0.82	0.87	0.88	0.74	0.78	0.84	0.82
LS-4	0.81	0.84	0.87	0.74	0.77	0.84	0.81
LS-5	0.78	0.84	0.86	0.67	0.74	0.83	0.79
LS-6	0.84	0.86	0.88	0.73	0.77	0.84	0.82
LS-7	0.81	0.85	0.88	0.77	0.79	0.85	0.83
LS-8	0.80	0.85	0.87	0.73	0.77	0.83	0.81
LRG-1	0.86	0.87	0.90	0.82	0.84	0.87	0.86
LRG-2	0.86	0.89	0.85	0.74	0.78	0.84	0.83
LRG-3	0.85	0.88	0.91	0.82	0.84	0.87	0.86
LRG-4	0.87	0.87	0.89	0.82	0.84	0.86	0.86
LRG-5	0.84	0.87	0.90	0.81	0.83	0.87	0.85
RG-1	0.85	0.87	0.89	0.71	0.75	0.84	0.82
RG-2	0.88	0.88	0.90	0.81	0.83	0.86	0.86
RG-3	0.86	0.87	0.89	0.80	0.83	0.86	0.85
DOL-1	0.79	0.85	0.87	0.71	0.75	0.83	0.80
DOL-2	0.79	0.83	0.85	0.75	0.79	0.83	0.81
DOL-3	0.79	0.84	0.85	0.74	0.78	0.84	0.81
CRG-1	0.88	0.88	0.90	0.81	0.82	0.85	0.86
CRG-1	0.83	0.87	0.90	0.81	0.83	0.87	0.85
TR-1	0.79	0.84	0.88	0.74	0.76	0.83	0.81
TR-2	0.81	0.82	0.84	0.76	0.80	0.84	0.81
GR	0.78	0.83	0.85	0.72	0.75	0.81	0.79
SS	0.81	0.84	0.87	0.71	0.70	0.81	0.79

Table B.7: Camsizer Symmetry Results

Designation	No. 8	No. 16	No. 30	No. 50	No. 100	No. 200	Average
LS-1	0.87	0.88	0.87	0.84	0.83	0.86	0.86
LS-2	0.87	0.88	0.87	0.86	0.85	0.86	0.86
LS-3	0.88	0.89	0.87	0.85	0.85	0.86	0.87
LS-4	0.87	0.88	0.87	0.86	0.86	0.85	0.86
LS-5	0.87	0.88	0.86	0.84	0.84	0.84	0.86
LS-6	0.88	0.88	0.87	0.84	0.84	0.86	0.86
LS-7	0.88	0.88	0.87	0.87	0.86	0.86	0.87
LS-8	0.87	0.88	0.87	0.85	0.85	0.85	0.86
LRG-1	0.90	0.89	0.88	0.89	0.89	0.87	0.88
LRG-2	0.87	0.87	0.86	0.86	0.86	0.86	0.86
LRG-3	0.90	0.89	0.88	0.89	0.88	0.87	0.88
LRG-4	0.90	0.89	0.88	0.89	0.88	0.87	0.88
LRG-5	0.90	0.89	0.88	0.89	0.88	0.87	0.88
RG-1	0.90	0.88	0.87	0.89	0.88	0.86	0.88
RG-2	0.90	0.89	0.88	0.89	0.89	0.87	0.88
RG-3	0.90	0.89	0.88	0.88	0.88	0.87	0.88
DOL-1	0.87	0.88	0.87	0.84	0.83	0.85	0.86
DOL-2	0.86	0.87	0.86	0.86	0.86	0.86	0.86
DOL-3	0.87	0.87	0.86	0.86	0.86	0.86	0.86
CRG-1	0.89	0.89	0.88	0.89	0.89	0.87	0.88
CRG-1	0.90	0.88	0.87	0.89	0.88	0.87	0.88
TR-1	0.87	0.88	0.87	0.86	0.84	0.85	0.86
TR-2	0.87	0.87	0.86	0.87	0.87	0.86	0.86
GR	0.87	0.87	0.86	0.86	0.85	0.85	0.86
SS	0.87	0.88	0.87	0.85	0.81	0.84	0.85

Table B.8: Uncompacted Void Content Test Results

Designation	Method A	Method B	Method C
LS-1	48.52	53.26	42.77
LS-2	43.11	48.22	38.58
LS-3	48.38	53.07	46.18
LS-4	46.47	51.60	42.91
LS-5	48.37	52.95	41.79
LS-6	44.96	50.05	41.32
LS-7	44.85	48.64	42.77
LS-8	45.38	50.15	40.72
LRG-1	39.85	45.11	38.22
LRG-2	38.24	43.82	35.65
LRG-3	38.71	43.28	37.77
LRG-4	39.81	45.19	36.18
LRG-5	37.85	43.81	35.17
RG-1	41.00	44.61	39.92
RG-2	39.69	43.15	36.85
RG-3	41.22	45.06	39.50
DOL-1	45.68	50.43	38.18
DOL-2	47.66	52.27	44.53
DOL-3	46.80	51.68	41.35
CRG-1	41.06	44.14	39.54
CRG-1	41.98	45.42	43.99
TR-1	51.95	55.70	45.71
TR-2	48.83	53.58	46.40
GR	47.49	51.35	43.63
SS	46.95	51.46	40.08

Table B.9: Mortar Flow Test Results of Fine Aggregates

Designation	As-received Grading	Standard Grading
LS-1	60	50
LS-2	117	122
LS-3	76	98
LS-4	85	98
LS-5	113	121
LS-6	78	108
LS-7	68	102
LS-8	128	104
LRG-1	151	150
LRG-2	128	160
LRG-3	138	160
LRG-4	142	152
LRG-5	134	160
RG-1	142	160
RG-2	148	160
RG-3	131	160
DOL-1	145	142
DOL-2	104	133
DOL-3	134	138
CRG-1	149	150
CRG-1	108	140
TR-1	55	128
TR-2	114	148
GR	113	130
SS	86	84

Table B.10: Compressive strength Results of Fine Aggregates

Designation	As-received Grading (psi)	Standard Grading (psi)
LS-1	6899	6566
LS-2	6218	6779
LS-3	1605	2223
LS-4	6813	6546
LS-5	6490	6487
LS-6	5201	6236
LS-7	6634	7281
LS-8	6715	6705
LRG-1	4768	6254
LRG-2	6444	6297
LRG-3	5458	6032
LRG-4	5565	5721
LRG-5	5943	5853
RG-1	5123	5313
RG-2	5123	6963
RG-3	6367	6366
DOL-1	5909	7155
DOL-2	6243	7343
DOL-3	6596	6496
CRG-1	6078	6970
CRG-1	5246	4328
TR-1	6915	7778
TR-2	7128	5950
GR	6668	5869
SS	8035	7858

Table B.11: Form 2-D (BMD) Results

Designation	No. 8	No. 16	No. 30	No. 50	No. 100	No. 200	Average
LS-1	7.25	7.23	7.09	6.90	6.13	8.32	7.25
LS-2	7.54	7.87	7.24	7.04	6.77	7.36	7.54
LS-3	7.25	6.98	6.52	6.27	5.73	7.54	7.25
LS-4	7.33	7.60	7.15	6.36	6.84	7.66	7.33
LS-5	7.08	7.71	7.09	6.79	6.41	7.89	7.08
LS-6	6.65	7.54	6.69	6.81	6.35	7.68	6.65
LS-7	7.26	7.72	7.20	6.63	6.01	7.44	7.26
LS-8	7.32	7.86	7.66	7.50	6.02	7.60	7.32
LRG-1	6.43	6.55	6.15	6.14	5.99	7.62	6.43
LRG-2	6.14	6.24	5.45	5.43	5.95	7.46	6.14
LRG-3	6.43	6.46	6.02	5.72	6.51	7.87	6.43
LRG-4	6.38	6.39	6.72	6.61	6.19	7.51	6.38
LRG-5	6.16	6.40	5.90	5.95	6.31	8.00	6.16
RG-1	6.53	6.50	6.45	6.21	6.54	7.79	6.53
RG-2	5.80	6.96	6.70	5.70	5.94	7.88	5.80
RG-3	6.25	6.51	6.24	6.22	6.26	8.41	6.25
DOL-1	7.40	7.51	7.27	6.47	6.39	7.81	7.40
DOL-2	7.39	8.05	8.00	7.58	6.63	7.67	7.39
DOL-3	7.50	7.76	7.48	7.29	7.15	8.83	7.50
CRG-1	5.95	6.18	6.02	6.17	6.56	8.28	5.95
CRG-1	7.02	6.98	6.24	6.03	6.39	7.17	7.02
TR-1	-	-	-	-	-	-	-
TR-2	-	-	-	-	-	-	-
GR	8.17	8.30	8.32	8.70	8.28	8.28	8.17
SS	7.85	8.24	8.18	7.30	7.08	7.87	7.85

Table B.12: Form 2-D (AMD) Results

Designation	No. 8	No. 16	No. 30	No. 50	No. 100	No. 200	Average
LS-1	7.25	7.23	7.09	6.90	6.13	8.32	7.25
LS-2	7.54	7.87	7.24	7.04	6.77	7.36	7.54
LS-3	7.25	6.98	6.52	6.27	5.73	7.54	7.25
LS-4	7.33	7.60	7.15	6.36	6.84	7.66	7.33
LS-5	7.08	7.71	7.09	6.79	6.41	7.89	7.08
LS-6	6.65	7.54	6.69	6.81	6.35	7.68	6.65
LS-7	7.26	7.72	7.20	6.63	6.01	7.44	7.26
LS-8	7.32	7.86	7.66	7.50	6.02	7.60	7.32
LRG-1	6.43	6.55	6.15	6.14	5.99	7.62	6.43
LRG-2	6.14	6.24	5.45	5.43	5.95	7.46	6.14
LRG-3	6.43	6.46	6.02	5.72	6.51	7.87	6.43
LRG-4	6.38	6.39	6.72	6.61	6.19	7.51	6.38
LRG-5	6.16	6.40	5.90	5.95	6.31	8.00	6.16
RG-1	6.53	6.50	6.45	6.21	6.54	7.79	6.53
RG-2	5.80	6.96	6.70	5.70	5.94	7.88	5.80
RG-3	6.25	6.51	6.24	6.22	6.26	8.41	6.25
DOL-1	7.40	7.51	7.27	6.47	6.39	7.81	7.40
DOL-2	7.39	8.05	8.00	7.58	6.63	7.67	7.39
DOL-3	7.50	7.76	7.48	7.29	7.15	8.83	7.50
CRG-1	5.95	6.18	6.02	6.17	6.56	8.28	5.95
CRG-1	7.02	6.98	6.24	6.03	6.39	7.17	7.02
TR-1	-	-	-	-	-	-	-
TR-2	-	-	-	-	-	-	-
GR	8.17	8.30	8.32	8.70	8.28	8.28	8.17
SS	7.85	8.24	8.18	7.30	7.08	7.87	7.85

Table B.13: Angularity (BMD) Results

Designation	No. 8	No. 16	No. 30	No. 50	No. 100	No. 200	Average
LS-1	3245.8	3229.2	3243.6	3094.7	1916.9	1745.4	2745.9
LS-2	3206.9	3595.9	3426.5	3253.5	2355.5	1495.7	2889.0
LS-3	3241.8	3036.3	3113.9	2748.7	1948.2	1359.5	2574.7
LS-4	3234.4	3360.0	3089.2	2745.9	2240.8	1379.4	2675.0
LS-5	3453.5	3414.3	3320.5	2950.5	2218.1	1588.0	2824.2
LS-6	2941.7	3060.0	2966.0	2503.1	1871.5	1500.5	2473.8
LS-7	3184.6	3276.2	2969.9	2394.1	1833.7	1504.2	2527.1
LS-8	3657.9	3600.6	3386.1	3394.0	1605.4	1493.0	2856.1
LRG-1	2461.0	2747.2	2308.5	2260.8	1894.7	1587.5	2210.0
LRG-2	4008.3	4370.1	2279.6	2859.4	1768.3	1455.0	2790.1
LRG-3	2348.1	2429.9	2393.4	2205.0	2315.3	1792.4	2247.4
LRG-4	2534.1	2646.1	2854.2	2604.3	2034.8	1686.3	2393.3
LRG-5	2137.1	2448.8	2384.6	2100.6	1980.6	1661.7	2118.9
RG-1	2670.6	2976.7	2886.9	2602.8	2410.8	1841.4	2564.9
RG-2	2724.1	2836.5	2634.0	2189.3	1989.5	1747.6	2353.5
RG-3	2762.1	2943.6	2770.3	2476.6	2159.5	2009.2	2520.2
DOL-1	3357.7	3378.1	3353.1	2769.1	2273.1	1601.2	2788.7
DOL-2	3251.6	3374.9	3286.5	2915.6	2138.7	1664.1	2771.9
DOL-3	3799.4	3702.8	3580.5	3132.9	2404.0	2032.5	3108.7
CRG-1	2773.0	2734.3	2626.4	2612.3	2336.7	2059.5	2523.7
CRG-1	3090.1	3320.1	2443.1	2286.3	2075.3	1455.7	2445.1
TR-1	-	-	-	-	-	-	-
TR-2	-	-	-	-	-	-	-
GR	4138.4	3933.9	3533.8	3322.2	2730.2	2169.2	3304.6
SS	3598.3	3764.4	3874.2	3677.1	2769.0	1776.9	3243.3

Table B.14: Angularity (AMD) Results

Designation	No. 8	No. 16	No. 30	No. 50	No. 100	No. 200	Average
LS-1	2969.8	2987.3	3013.9	2601.9	1978.6	1660.9	2535.4
LS-2	2816.4	2968.8	2931.5	2329.3	2142.7	1456.0	2440.8
LS-3	2821.2	3256.5	2825.3	2584.5	2068.4	1394.3	2491.7
LS-4	3076.3	3017.1	2884.4	2431.8	1880.7	1412.2	2450.4
LS-5	3063.2	3072.6	2925.6	2538.2	2088.4	1532.1	2536.7
LS-6	2804.5	2813.8	2726.7	2260.2	1950.4	1456.3	2335.3
LS-7	3189.3	2982.3	2865.7	2558.6	1872.6	1604.9	2512.2
LS-8	3645.9	3565.6	3027.0	2717.2	2286.6	1853.8	2849.3
LRG-1	2381.1	2402.2	2375.0	2330.0	2226.4	1825.3	2256.7
LRG-2	2337.5	2243.4	2279.6	2350.7	2026.1	1745.4	2163.8
LRG-3	2188.2	2395.7	2349.5	2536.0	2485.4	1846.4	2300.2
LRG-4	2637.4	2506.8	2890.0	2647.8	2497.4	1796.1	2495.9
LRG-5	2221.0	2547.5	2331.6	2198.9	2245.6	1546.7	2181.9
RG-1	2588.4	2884.3	2869.8	2680.4	2522.4	1650.8	2532.7
RG-2	2598.4	2935.3	2660.7	2615.3	2503.1	1788.1	2516.8
RG-3	2691.1	2723.2	2791.4	2597.9	2533.5	2093.0	2571.7
DOL-1	3001.7	3146.0	3171.6	2646.3	2295.3	1817.0	2679.7
DOL-2	3106.6	3101.4	2863.6	2563.2	2178.7	1766.6	2596.7
DOL-3	3535.2	3610.7	3240.2	2909.1	2161.2	1933.7	2898.4
CRG-1	2862.2	2814.0	2803.8	2581.8	2649.2	2172.9	2647.3
CRG-1	3134.1	3016.7	2588.4	2716.0	2076.0	1678.8	2535.0
TR-1	-	-	-	-	-	-	-
TR-2	-	-	-	-	-	-	-
GR	4101.9	3764.1	3459.2	3242.6	2817.3	2409.3	3299.1
SS	3688.6	3736.6	3734.8	3471.6	2537.6	2196.9	3227.7

References

ASTM Standard C 136, 2006, "*Standard Test Method for Sieve Analysis of Fine and Coarse Aggregates*," ASTM International, West Conshohocken, PA, 2006, www.astm.org.

ASTM Standard C 1252, 2006, "*Standard Test Methods for Uncompacted Void Content of Fine Aggregate (as Influenced by Particle Shape, Surface Texture, and Grading),*" ASTM International, West Conshohocken, PA, 2006, www.astm.org.

ASTM Standard C 1252, 2006, "*Standard Test Methods for Uncompacted Void Content of Fine Aggregate (as Influenced by Particle Shape, Surface Texture, and Grading),*" ASTM International, West Conshohocken, PA, 2006, www.astm.org.

ASTM Standard C109/C109M, 2012, "*Standard Test Method for Compressive Strength of Hydraulic Cement Mortars (Using 2-in. or [50-mm] Cube Specimens),*" ASTM International, West Conshohocken, PA, 2012, www.astm.org.

ASTM Standard C 1437, 2007 *"Standard Test Method for Flow of Hydraulic Cement Mortar,*" ASTM International, West Conshohocken, PA, 2007, www.astm.org.

ASTM Standard D 7428, 2008 *"Standard Test Method for Resistance of Fine Aggregate to Degradation by Abrasion in the Micro-Deval Apparatus,*" ASTM International, West Conshohocken, PA, 2008, www.astm.org.

ASTM Standard C 837, 2009 *"Standard Test Method for Methylene Blue Index of Clay,*" ASTM International, West Conshohocken, PA, 2009, www.astm.org.

ASTM Standard D 2419, 2009 *"Standard Test Method for Sand Equivalent Value of Soils and Fine Aggregate,*" ASTM International, West Conshohocken, PA, 2009, www.astm.org.

AASHTO Standard TP 81, 2012 *"Standard Method of Test forDetermining Aggregate Shape Properties by Means of Digital Image Analysis,*" AASHTO International, Washington, D.C, 2012, http://www.transportation.org.

Al-Rousan, T., Masad, E., Myers, L., and Speigelman, C. (2006, December 28). New methodology for shape classification of aggregates. *Transportation Research Record: Journal of the Transportation Research Board, 1913*(1), 11 - 23.

doi:10.3141/1913-02

Harini, M., Shaalini, G., and Dhinakaran, G. (2011, April 15). Effect of size and type of fine aggregates on flowability of mortar. *KSCE Journal of Civil Engineering , 16*(1), 163-168. doi:10.1007/s12205-012-1283-4

Hu, J., and Wang, K. (2007, March 2). Evaluation of compacted aggregate resistant test compared with the fine aggregate angularity standards. *Journal of Advanced Concrete Technology, 5*(1), 75 - 85. doi:10.3151/jact.5.75

Kuo, C.-Y., and Freeman, R. (2007, January 24). Imaging indices for Quantification of shape, angularity, and surface texture of aggregates. *Transportation Research Record: Journal of the Transportation Research Board, 1721*(1), 57-65. doi:10.3141/1721-07

Kuo, C.-Y., and Freeman, R. (2007, January 30). Image analysis evaluation of aggregates for asphalt concrete mixtures. *Transportation Research Record: Journal of the Transportation Research Board, 1615*(1), 65 - 71. doi:10.3141/1615-09

Mahmoud, E., Gates, L., Masad, E., Erdogan, S., and Garboczi, E. (2010, April 4). Comprehensive evaluation of AIMS texture, angularity, and dimension measurements. *Journal of Materials in Civil Engineering, 22*(4), 369 - 379. doi:10.1061/(ASCE)MT.1943-5533.0000033

Masad, E., Al-Rousan, T., Button, J., Little, D., and Tutumluer, E. (2007). *Test methods for characterizing aggregate shape, texture, and angularity* (Rep. No. 555). Washington: National Cooperative Highway Research Program
.

Muszynski, M. R., and Vitton, S. J. (2012, January 17). Particle shape estimates of uniform sands: visual and automated methods comparison. *Journal of Materials in Civil Engineering, 24*(12), 194 - 206. doi:10.1061/(ASCE)MT.1943-5533.0000351

Topal, A., & Sengoz, B. (2008, May 5). Evaluation of compacted aggregate resistant test compared with the fine aggregate angularity standards. *Construction and Building Materials, 22*(5), 163-168. doi:10.1016/j.conbuildmat.2006.11.016

Wang, L., Wang, X., Mohammad, L., and Abadie, C. (2005, October). Unified method to quantify aggregate shape angularity and texture using Fourier analysis.

Journal of Materials in Civil Engineering, 17(5), 498–504. doi:10.1061/(ASCE)0899-1561(2005)17:5(498)

Wilson, M. L., and Kosmatka, S. H. (n.d.). *Design and Control of Concrete Mixtures* (15th ed.). Portland Cement Assn. (Original work published 2011). doi:978-0853342540

Newman, J., and Choo, B. S. (2003). *Advanced concrete technology 1: Constituent* materials (Vol. 1). Spon Press. (Original work published 2003). doi:978-0853342540

Maxwell, L. G. (1986). *Handbook of Road Technology* (4th ed.). Spon Press. (Original work published 2009). doi:978-0853342540

Masad, E., Al-Rousan, T., Button, J., Little, D., and Tutumluer, E. (2007). *Test methods for characterizing aggregate shape, texture, and angularity* (Rep. No. 555). Washington: National Cooperative Highway Research Program.

Hampel, K. W. (2005). *Predicting coarse aggregate performance using the Micro-Deval test with strength and intrinsic particle property tests* (Unpublished master's thesis). The University of Texas at Austin.

Rogers and Gorman Tutumluer, E. (2009). *A Flakiness Test for Fine Aggregate* (Rep. No. 034). Ontario: Ontario Ministry of Transportation.

Vita

Ali Saeed Alqarni was born in Riyadh, Saudi Arabia, on August 03, 1986. After completing his work at Jareer High School, Riyadh, Saudi Arabia in 2005. He entered King Saud University in Riyadh, Saudi Arabia. He participated in many engineering activities during the summers of his undergraduate study. He was also employed part-time for a structural design office in Riyadh during school. He received the degree of Bachelor of Science from King Saud University in June, 2009. He was appointed as teaching assistant at King Saud University. He was rewarded a scholarship to pursue his graduate studies. He entered The University of Texas at Austin in January, 2012 to pursue a Master of Science in Engineering degree in materials engineering through the Department of Civil, Architectural and Environmental. He graduated from The University of Texas at Austin in August 2013.